



ISSN: 2330-7609

Volume 11 Number 4 December 2023

<http://www.sciencepublishinggroup.com/j/hyd>

Hydrology

Science Publishing Group, USA

Hydrology

ISSN: 2330-7609 (PRINT) ISSN: 2330-7617 (ONLINE)

<http://www.sciencepublishinggroup.com/j/hyd>

Editorial Board

(For more editorial members, please refer to online information)

Dr. Xuezhi Tan	Department of Civil Engineering, Sun Yat-sen University, Guangzhou, China
Qinli Yang	School of Resources and Environment, University of Electronic Science and Technology of China, Chengdu, China
Dr. P. Manju Sree	Advanced Analytics Division, Remote Sensing Applications Area, National Remote Sensing Centre, Indian Space Research Organisation, Hyderabad, India
Dr. Mohammed Bari	Science and Innovation Group, Australian Bureau of Meteorology, West Perth, Australia
Dr. Pushendra Kumar Singh	Department of Water Resources System, National Institute of Hydrology, Roorkee, India
Sirisha Adamala	Department of Natural Resources Management, Indian Council of Agricultural Research-Central Inland Agricultural Research Institute, Port Blair, India
Dr. Vinay Rangari	Department of Civil Engineering, Nanasaheb Mahadik College of Engineering, Peth, India
Leila Rahimi	Department of Civil and Environmental Engineering, Politecnico di Milano, Milan, Italy
Ripendra Awal	College of Agriculture and Human Sciences, Prairie View A&M University, Prairie View, United States
Dr. Jichao Sun	School of Water Resource & Environment, China University of Geosciences (Beijing), Beijing, China
Qingwei Zhuang	State Key Laboratory of Information Engineering in Surveying, Mapping and Remote Sensing, Wuhan University, Wuhan, China
Dr. Mohammad Rizwan	Department of Geology, Vikram University, Ujjain, India
Jiefeng Wu	School of Hydrology and Water Resources, Nanjing University of Information Science and Technology, Nanjing, China
Sabab Ali Shah	Department of Civil and Environmental Engineering, Hanyang University, Seoul, South Korea
Yuhong Li	School of Civil and Hydraulic Engineering, Huazhong University of Science and Technology, Wuhan, China
Dr. Sonam Sandeep Dash	School of Civil Engineering, University College Dublin, Dublin, Ireland
Poojashree B. P.	Department of Marine Geology, Mangalore University, Mangaluru, India
Yuzhen Li	School of Emergency Management, Xihua University, Chengdu, China

CONTENTS

Vol. 11 No. 4

December 2023

Deficit Irrigation and Mulching Impacts on Major Crop Yield and Water Efficiency: A Review

Zalalem Tamiru Bekele, Addisu Asefa Mengasha 62

Analysis of Electrical Resistivity Survey Data for Aquifer Potential and Protective Capacity at Mararaba Dan-Daudu Minna, North Central Nigeria

Alfa Idris Alhaji, Salako Kazeem Adeyinka, Rafiu Abdulwaheed Adewuyi, Udensi Emmanuel Emeka, Adetona Abbas Adebayo, Jamilu Shehu 67

General Extreme Value Fitted Rainfall Non-Stationary Intensity-Duration-Frequency (NS-IDF) Modelling for Establishing Climate Change in Benin City

Masi G. Sam, Ify L. Nwaogazie, Chiedozie Ikebude 85

Hydrology (HYD)

JOURNAL INFORMATION

Hydrology (HYD) is published quarterly by Science Publishing Group (SciencePG), online at <http://www.sciencepublishinggroup.com/j/hyd>

SUBMISSION

To submit, please visit: <http://www.sciencepublishinggroup.com/login>
Any questions, just contact: journal@sciencepublishinggroup.com

REPRINTS

Reprints of the published journal are issued by SciencePG.
Cost: 100USD/one hard copy.
E-mail: journal@sciencepublishinggroup.com

ADVANTAGES

Peer Review

All papers submitted to journals in SciencePG are peer-reviewed.

Fast Publication

Papers of good quality can be published within two months after being submitted to SciencePG.

High Visibility

Each journal in SciencePG uses the OpenURL standard, making it easy for libraries to link users as directly as possible from citation to the full text of the article.

Open Access

Open Access makes knowledge available to all, without the barrier of affordability and without restrictions on using it to develop related areas of research.

Abstracting and Indexing

WorldCat, CrossRef, JournalSeek, Academickeys, ResearchBib, Directory of Research Journals Indexing (DRJI) and others.

COPYRIGHT

The authors' publications in SciencePG are distributed under Creative Commons Attribution (CC BY) license (<http://creativecommons.org/licenses/by/4.0/>). The license was developed to facilitate open access, namely, free immediate access to and unrestricted reuse of original works of all types.

Under this license, authors retain ownership of the copyright for their publications, but grant SciencePG a non-exclusive license to publish the work in paper form and allow anyone to reuse, distribute and reproduce the content as long as the original work is properly cited.

Appropriate attribution can be provided by simply citing the original work. No permission is required from the authors or the publishers. For any reuse or distribution of a work, users must also make clear the license terms under which the work was published.

The standard license will be applied to the authors' publications, which ensures the publications freely and openly available in perpetuity.

For more information contact us by

E-mail: service@sciencepublishinggroup.com

Review Article

Deficit Irrigation and Mulching Impacts on Major Crop Yield and Water Efficiency: A Review

Zalalem Tamiru Bekele^{*}, Addisu Asefa Mengasha^{*}

Jimma Agricultural Research Center, Jimma, Ethiopia

Email address:

zalalemt75@gmail.com (Zalalem Tamiru Bekele)

^{*}Corresponding author**To cite this article:**Zalalem Tamiru Bekele, Addisu Asefa Mengasha. Deficit Irrigation and Mulching Impacts on Major Crop Yield and Water Efficiency: A Review. *Hydrology*. Vol. 11, No. 4, 2023, pp. 62-66. doi: 10.11648/j.hyd.20231104.11**Received:** August 16, 2023; **Accepted:** September 7, 2023; **Published:** October 14, 2023

Abstract: The review examines the impact of deficit irrigation and mulching materials on crop yield and water use efficiency. The challenges posed by population growth and climate change necessitate new solutions to improve agriculture. The best irrigation strategies yield large yields for a given amount of water. Deficit irrigation and mulching significantly increase water use efficiency and crop yield for various crops. However, water supply constraints have led to the development of deficit irrigation; a strategy that maximizes water use efficiency without yield penalty. Mulch is a vital method for conserving soil moisture, preventing weed growth, reducing evaporation, and increasing infiltration of rainwater during the growing season. Different mulching methods and materials are used worldwide, with plastic and straw being the most popular and optimistic results. Straw mulch conserves higher soil moisture by 55% more compared to the control, and crops under straw mulch produce higher branches, fruit weight, and total yield. Polyethylene mulches have induced large increases in growth and yields for various vegetables, including tomato. However, the economic profitability of this mulch is low, so straw mulch is better for economic profitability. Plastic cover ridge furrow methods are better for increasing water use efficiency (WUE) and crop yield, reducing soil evaporation and erosion, increasing top soil temperature, creating a microenvironment for soil microbial activity, and increasing sustainability.

Keywords: Deficit Irrigation, Mulching, Water Use Efficiency

1. Introduction

Water shortages caused by population expansion and irregular precipitation increase agriculture's demand, necessitating new solutions for sustainable agriculture. Cooperative irrigation management aims to maximize water use efficiency and maintain soil moisture for plants [1]. Producers adopt time deficit irrigation to achieve high yields without reaching field capacity. Mulching and deficit irrigation are strategies to decrease water use in agriculture, benefiting crop production and yield, especially under low water availability. This reduces the frequency of phytosanitary measures and production costs [1, 2].

1.1. Irrigation Deficit

Conventional irrigation development focuses on avoiding water deficits to achieve maximum yields [3]. However, water

supply constraints have led to the development of DI, a strategy that maximizes water use efficiency without yield penalty [4, 5]. DI requires detailed irrigation management and identifies crop characteristics and stress-related yield come backs [6]. DI involves applying water below optimal evapotranspiration levels, reducing water use while minimizing adverse impacts on yield [7]. It aims to stabilize yields and achieve maximum crop water productivity, improving water productivity and reducing irrigation application [50].

1.2. Water Use Efficiency

Water use efficiency (WUE) is a concept that compares crop production to water usage. The best irrigation strategies produce a large yield for a given amount of irrigation [8]. Producers often aim to increase profits, but determining the

level of irrigation needed can be complex and depends on biophysical and economic factors [9]. WUE is the main criterion for evaluating production systems in areas with limited water resources, where water is the greatest limitation to production [10, 11].

1.3. Mulching

Mulching is an in-situ moisture preservation system that maintains soil moisture, reduces weed growth, and mitigates erosion. It improves crop yield and water use efficiency [12]. The degree of drop between mulch and soil affects soil warming [13].

1.4. Soil Moisture Management

Soil and water-management systems aim to encourage water infiltration, but often fail to optimize water flow along crop rooting zones, leading to poor yields due to soil moisture insufficiency rather than rainfall insufficiency [31]. Proper moisture conservation is crucial, as moisture deficits can severely depress crop yields, while adequate management can increase yields by a factor two or more [6].

1.5. Water Saved

Mulching is a water-saving technique in dryland areas that conserves soil moisture, regulates temperature, and reduces evaporation [14-16]. Its main strength is reducing surface evaporation and controlling soil erosion). Mulching decreases irrigation demand during crop cultivation periods by reducing soil evaporation and regulating temperature [16-18]. The amount of water saved by mulching is critical due to the interaction of microclimate, soil environment, and plant growths [19].

1.6. Retains Moisture

Organic and non-organic mulches cover soil, limit evaporation, absorb water, and retain moisture for plant growth. They help reduce water bills during hot and humid summers, providing water for plants and reducing physical water requirements for gardens.

2. Results and Discussion

Effect of Deficit Irrigation and Mulches on Water Use Efficiency and Crop Yield

Mulch is a crucial method for conserving soil moisture, as it helps prevent weed growth, reduce evaporation, and increase infiltration of rainwater during the growing season. Plastic mulch helps prevent soil water loss during dry years and sheds excessive water away from the crop root zone during periods of excessive rain fall. This can reduce irrigation frequency and amount of water, and may help reduce the incidence of moisture-related physiological disorders such as blossom end rot on vegetables and fruit cracking in lime and pomegranate [20]. Mulch provides numerous benefits to crop production through soil and water conservation, enhanced soil biological activity, and improved chemical and physical properties of the

soil. Studies have shown that mulches conserve more soil moisture, enhance vegetative growth and yield-committing characteristics of garlic [21-23]. Crop residues or mulch at the soil surface act as shade and serve as a vapour barrier against moisture losses from the soil, causing slow surface runoff. Straw mulch conserves higher soil moisture to an extent of 55% more compared to the control. Crop under straw mulch produced higher number of branches, fruit weight, and total yield compared to no mulch [24]. Polyethylene mulches have induced large increases in growth and yields for various vegetables, including tomato [26-29]. These increases have been attributed to changes in soil and air temperature near the cover, soil water balance, and nutrient availability compared to un mulched soil [30-33]. Less soil compaction and improved aeration under mulched soil have also contributed to increased plant growth [34]. In situations where water productivity is increased, priority for polyethylene mulch may be the option. However, the economic profitability of this mulch is low, so it is better to use straw mulch for economic profitability [35].

Table 1. Influence of water regimes on tuber yield of potato for mulched (M) and non-mulched (NM) plots.

Water level	Tuber yield t/ha				
	100%	90%	80%	60%	50%
Mulch	31.5	29.6	28.9	26.9	23.2
Non Mulch	28.3	25.8	24.9	21.9	20.3

Source [36].

The study found that half mulched maize straw yielded the highest grain yield and water use efficiency. However, this pattern was more favorable for wheat growth, soil temperature, and water efficiency. Plastic cover ridge furrow methods are better for increasing water use efficiency (WUE) and crop yield. They also reduce soil evaporation and erosion in arid and semiarid conditions, increase top soil temperature, create a microenvironment for soil microbial activity, and increase sustainability [37].

Mulch enhances soil physical properties through aggregation, increased water content, and reduced runoff, leading to better germination and higher yield. It also increases nutrient availability to plant roots, leading to higher grain yield. Plastic mulch increases grain yield by 17% and above ground biomass by 19% [38]. The bed planting method of full irrigation with plastic mulching soil condition yields higher baby corn yield. The system also increases soil temperature, accelerates early growth, plant height, fruiting, and provides satisfactory weed control without herbicide application. In the top soil layer, mulching treatment significantly increases soil water content, with high nitrate-N content distributed. The yield increased with increased basal fertilizer, top dressing, and plastic film mulching, improving fertilizer use efficiency [39]. Plastic film mulching can be effectively utilized for improving productivity and water use efficiency in rice production [40]. Straw mulching reduces soil evaporation by 43mm for maize and WUE by over 10%, indicating that water use efficiency increases with the decrease in irrigation depth applied.

Plastic mulch has been shown to increase crop yield by improving solar energy, water, and fertility status, reducing soil water loss, and removing weeds [41-43]. This can lead to increased grain yield and water use efficiency (WUE). Mulching with plastic film has been shown to enhance water use efficiency by 14%, grain yield by 17%, and biological yield by 19%. The soil on top of mulch retains structural stability and lower bulk density compared to un-mulched soil, likely due to less structural disruption of aggregates and settlement in unsaturated conditions [49]. Plastic sheet mulch is more effective for conservation of soil water than that of wheat straw mulch [44]. Experiment conducted in Nigeria to study the effects of deficit irrigation and mulch on onion yield, water use, and crop water productivity [45]. Results showed that irrigating onion at 25% of weekly reference evapotranspiration reduced bulb yield by 50%. Applying water at 50% and 75% water requirements led to a 15.5-23% reduction in yield and higher water use efficiency. Yield reductions reported in 78%, 45%, and 15% when onion crop was irrigated at 25%, 50%, and 75% of ET_c [46]. Study found that onion bulb yield decreased with increasing water deficit levels, while both water use and irrigation water use efficiencies increased with water deficit levels [47, 48]. Deficit irrigation and mulch had significant positive impacts on growth parameters like plant height, scape length and diameter, and umbel diameter.

3. Conclusion

Mulch is a vital method for conserving soil moisture, preventing weed growth, reducing evaporation, and increasing infiltration of rainwater during the growing season. It also helps prevent soil water loss during dry years and sheds excessive water away from the crop root zone during periods of excessive rain fall. Mulch provides numerous benefits to crop production through soil and water conservation, enhanced soil biological activity, and improved chemical and physical properties of the soil. Studies have shown that mulches conserve more soil moisture, enhance vegetative growth, and yield-committing characteristics. Straw mulch conserves higher soil moisture by 55% more compared to the control, and crops under straw mulch produce higher branches, fruit weight, and total yield. Polyethylene mulches have induced large increases in growth and yields for various vegetables, including tomato. However, the economic profitability of this mulch is low, so straw mulch is better for economic profitability. Plastic cover ridge furrow methods are better for increasing water use efficiency (WUE) and crop yield, reducing soil evaporation and erosion, increasing top soil temperature, creating a microenvironment for soil microbial activity, and increasing sustainability.

References

- [1] Saraiva, K. R., VIANA, T. V. D. A., BEZERRA, F., LIMA, M., COSTA, S. C. and GONDIM, R. S., 2017. REGULATED DEFICIT IRRIGATION AND DIFFERENT MULCH TYPES ON FRUIT QUALITY AND YIELD OF WATERMELON1. *Revista Caatinga*, 30, pp. 437-446.
- [2] Lin, Z., LIU, J. L., LUO, S. S., BU, L. D., CHEN, X. P. and LI, S. Q., 2015. Soil mulching can mitigate soil water deficiency impacts on rainfed maize production in semiarid environments. *Journal of Integrative Agriculture*, 14 (1), pp. 58-66.
- [3] Doorenbos, J. and W. H. Pruitt. 1992. Crop water requirements. *FAO Irrigation and Drainage Paper Number 24*, FAO, Rome, Italy.
- [4] English, M. J., Solomon, K. H. and Hoffman, G. J., 2002. A paradigm shift in irrigation management. *Journal of irrigation and drainage engineering*, 128 (5), pp. 267-277.
- [5] Bouman, B. A. M., 2007. A conceptual framework for the improvement of crop water productivity at different spatial scales. *Agricultural systems*, 93 (1-3), pp. 43-60.
- [6] English, M. and Raja, S. N. 1996. Perspectives on deficit irrigation. *Agricultural Water Management*, 32 (1): 1-14.
- [7] Kirda, C., 2002. Deficit irrigation scheduling based on plant growth stages showing water stress tolerance. *Food and Agricultural Organization of the United Nations, Deficit Irrigation Practices, Water Reports*, 22 (102).
- [8] Mansouri-Far, C., Sanavy, S. A. M. M. and Saberali, S. F., 2010. Maize yield response to deficit irrigation during low-sensitive growth stages and nitrogen rate under semi-arid climatic conditions. *Agricultural Water Management*, 97 (1), pp. 12-22.
- [9] Payero, J. O., Tarkalson, D. D., Irmak, S., Davison, D. and Petersen, J. L., 2008. Effect of irrigation amounts applied with subsurface drip irrigation on corn evapotranspiration, yield, water use efficiency, and dry matter production in a semiarid climate. *Agricultural water management*, 95 (8), pp. 895-908.
- [10] Norton, N. A., Clark, R. T. and Schneckloth, J. P., 2000. Effects of alternative irrigation allocations on water use, net returns, and marginal user costs.
- [11] FAO (Food and Agriculture Organization). 2002. Deficit irrigation practice. *Water Reports Paper 22*. FAO, Rome, Italy.
- [12] Lamont, W. J., 1999. The use of different colored mulches for yield and earliness. In *Proceedings of the New England vegetable and berry growers conference and trade show, Sturbridge, Mass* (pp. 299-302).
- [13] Sweat, M., 2007. Plasticulture technology for vegetable production. *Institute of Food and Agricultural Sciences, North Florida Research and Education Center. Suwanee Valley (FL): University of Florida Cooperative Extension Service*. URL: <http://nfrec-sv.ifas.ufl.edu/mulch.htm> (accessed 10 Sep 2009).
- [14] Yang, N., Sun, Z. X., Feng, L. S., Zheng, M. Z., Chi, D. C., Meng, W. Z., Hou, Z. Y., Bai, W. and Li, K. Y., 2015. Plastic film mulching for water-efficient agricultural applications and degradable films materials development research. *Materials and Manufacturing Processes*, 30 (2), pp. 143-154.
- [15] Kader, M. A., Senge, M., Mojid, M. A. and Nakamura, K., 2017. Mulching type-induced soil moisture and temperature regimes and water use efficiency of soybean under rain-fed condition in central Japan. *International Soil and Water Conservation Research*, 5 (4), pp. 302-308.
- [16] Zribi, W., Aragüés, R., Medina, E. and Faci, J. M., 2015. Efficiency of inorganic and organic mulching materials for soil evaporation control. *Soil and Tillage Research*, 148, pp. 40-45.

- [17] Qin, S., Li, S., Kang, S., Du, T., Tong, L. and Ding, R., 2016. Can the drip irrigation under film mulch reduce crop evapotranspiration and save water under the sufficient irrigation condition?. *Agricultural Water Management*, 177, pp. 128-137.
- [18] Kader, M. A., Nakamura, K., Senge, M., Mojid, M. A. and Kawashima, S., 2019. Numerical simulation of water-and heat-flow regimes of mulched soil in rain-fed soybean field in central Japan. *Soil and Tillage Research*, 191, pp. 142-155.
- [19] Steinmetz, Z., Wollmann, C., Schaefer, M., Buchmann, C., David, J., Tröger, J., Muñoz, K., Frör, O. and Schaumann, G. E., 2016. Plastic mulching in agriculture. Trading short-term agronomic benefits for long-term soil degradation? *Science of the total environment*, 550, pp. 690-705.
- [20] Sangakkara, U. R., Attanayake, K. B., Gajanayake, J. N. and Bandaranayake, P. S. D. R., 2004, September. Impact of mulches on growth and yields of cassava and sweet potato in tropical Asia. In *New directions for a diverse planet: Proceedings of the 4th International Crop Science Congress Brisbane, Australia, Brisbane*.
- [21] Cooper, A. J., 1973. Root temperatures and plant growth. *Res. Rev. 4, Commonwealth Bureau of Horticulture and Plantation Crops*.
- [22] Menezes, S. M., Navais, D. E., Sontos, H. L. and Dos, M. A., 1974. The effect of nitrogen fertilization, plant spacing and mulching on the yield of garlic cultivar Amarante. *Revista Ceres*, 21, pp. 203-211.
- [23] Chung, H. D., 1987. Effects of PE film mulching, sulphur application and different levels of nitrogen and potassium on growth, flower-stalk elongation, bulbing, and leaf tip yellowing of garlic, *Allium sativum* L. cv. Euisung. *Han'guk Wonye Hakhoe chi= Journal of the Korean Society for Horticultural Science*.
- [24] Rathore, A. L., Pal, A. R. and Sahu, K. K., 1998. Tillage and mulching effects on water use, root growth and yield of rainfed mustard and chickpea grown after lowland rice. *Journal of the Science of Food and Agriculture*, 78 (2), pp. 149-161.
- [25] Chattha, T. H. and Hayat, R., 2005. Growth and Yield response of tomato (*Lycopersicon esculentum* L.) to organic and inorganic mulches. *Asian Journal of Plant Sciences*.
- [26] Takatori, F. H., Lippert, L. F. and Whiting, F. L., 1964. The effect of petroleum mulch and polyethylene films on soil temperature and plant growth. In *Proc. Am. Soc. Hort. Sci* (Vol. 85, pp. 532-540).
- [27] Vandenberg, J. and Tiessen, H., 1972. Influence of Wax-coated and Polyethylene-coated Paper Mulch on Growth and Flowering of Tomato 1. *HortScience*, 7 (5), pp. 464-465.
- [28] Mullins, C. A., Straw, R. A. and Rutledge, A. D., 1992. Tomato production with fertigation and black plastic mulch. *Tennessee farm and home science: progress report-Tennessee Agricultural Experiment Station (USA)*.
- [29] Lamont Jr, W. J., 2017. Plastic mulches for the production of vegetable crops. In *A guide to the manufacture, performance, and potential of plastics in agriculture* (pp. 45-60). Elsevier.
- [30] Clarkson, V. A., 1956. Effect of paper and polyethylene mulches and plastic caps on cantaloupe yields and earliness. In *American society for horticultural science* (Vol. 69, pp. 400-404).
- [31] Clarkson, V. A., 1960. Effect of black polyethylene mulch on soil and microclimate temperature and nitrate level. *Agronomy Journal*, 52 (6), pp. 307-309.
- [32] Brunini, O. and Santos, J. M. D., 1976. Estudo micrometeorológico com cenouras (var. nantes) I-Influência da temperatura do ar. *Bragantia*, 35, pp. 41-47.
- [33] Haynes, R. J., 1987. The use of polyethylene mulches to change soil microclimate as revealed by enzyme activity and biomass nitrogen, sulphur and phosphorus. *Biology and Fertility of soils*, 5, pp. 235-240.
- [34] Ekern, P. C., 1967. Soil Moisture and Soil Temperature Changes with the Use of Black Vapor-Barrier Mulch and Their Influence on Pineapple (*Ananas comosus* (L.) Merr.) Growth in Hawaii. *Soil Science Society of America Journal*, 31 (2), pp. 270-275.
- [35] Biswas, S. K., Sarker, P. K., Islam, A. M., Bhuiyan, M. A. and Kundu, B. C., 2003. Effect of irrigation on onion production. *Pakistan Journal of Biological Sciences (Pakistan)*.
- [36] Kiptoo, S., Kipkorir, E. C. and Kiptum, C. K., 2018. Effects of deficit irrigation and mulch on yield and quality of potato crop.
- [37] Memon, M. S., Zhou, J., Guo, J., Ullah, F., Hassan, M., Ara, S. and Ji, C., 2017. Comprehensive review for the effects of ridge furrow plastic mulching on crop yield and water use efficiency under different crops. *Int Agri Eng J*, 26 (2), pp. 58-67.
- [38] Gulshan Mahajan, Rakesh Sharda, Ashwani Kumar and K. G. Singh Effect of plastic mulch on economizing irrigation water and weed control in baby corn sown by different methods *African Journal of Agricultural Research* Vol. 2 (1), pp. 019-026, (2007).
- [39] Wang X, Xing Y. 2016 Effects of mulching and nitrogen on soil nitrate -N distribution, Leaching and Nitrogen Use efficiency of maize (*zeamays* L.). *PLoS ONE* 11 (8).
- [40] T. Oweis, M. Pala, J. Ryan. Stabilizing rainfed wheat yields with supplemental irrigation and nitrogen in a Mediterranean climate, *Agronomy Journal*, Vol. 20, 672-681, 1998.
- [41] Shahid, M. S. I. Zamir, T. Rasool and W. Akbar. 2014. Effect of tillage and mulching on soil fertility and grain yield of sorghum. *Sci. Agri*. 4: 31-36.
- [42] Zohaib, A., Ehsanullah, T. Tabassum, T. Abbas and T. Rasool. 2014. Influence of water soluble phenolics of *Vicia sativa* L. on germination and seedling growth of pulse crops. *Sci. Agri*. 8: 148-151.
- [43] Bu, Y. S., H. L. Shao and J. C. Wang. 2002. Effects of different mulch materials on corn seeding growth and soil nutrients contents and distributions. *J. Soil Water Conserv*. 16: 40-42.
- [44] Li R, Hou X, Jia Z, Han Q, Ren X, Yang B (2013) Effects on soil temperature, moisture, and maize yield of cultivation with ridge and furrow mulching in the rainfed area of the Loess Plateau, China. *Agric Water Manag* [Internet]. 116: 101-109.
- [45] Igbadun, H. E., A. A. Ramalan and E. Oiganji. 2012. Effects of regulated deficit irrigation and mulch on yield, water use and crop water productivity of onion in Samaru, Nigeria. *Journal of Agricultural Water Management*, 109: 162-169.
- [46] Bekele Samson and Tilahun Ketema. 2007. Regulated deficit irrigation scheduling of onion in a semi-arid region of Ethiopia. *Journal of Agricultural Water Management*, 89: 148-152.

- [47] Ramalan, A. A., Nega, H. and Oyeboode, M. 2010. Effect of deficit irrigation and mulch on water use and yield of drip irrigated onions. *WIT Trans Ecological Environ*, 134: 3950.
- [48] Bhagyawant, R. G., S. D. Gorantiwar, S. D. Dahiwalkar, M. N. Bhalekar, and D. D. Khedkar. 2014. Effect of deficit irrigation on growth, yield and quality of onion. *Bionfolet*, 11: 341-43.
- [49] Mehmood, S., T. Rasool, M. Iqbal, M. Iqbal, I. Haq and M. Sohail. 2015. Effect of plastic mulch and different irrigation practices on soil properties, nutrient contents and their availability in Maize. *Journal of Environmental & Agricultural Sciences*. 3: 35-41.
- [50] Zhang, H., Pala, M., Oweis, T., Harris, H. 2000. Water use and water use efficiency of chickpea and lentil in a Mediterranean environment. *Australian Journal of Agricultural Research*. 51, 295–305.

Analysis of Electrical Resistivity Survey Data for Aquifer Potential and Protective Capacity at Mararaba Dan-Daudu Minna, North Central Nigeria

Alfa Idris Alhaji¹, Salako Kazeem Adeyinka², Rafiu Abdulwaheed Adewuyi²,
Udensi Emmanuel Emeka², Adetona Abbas Adebayo^{2, *}, Jamilu Shehu²

¹Department of Physics, School of Sciences, Niger State College of Education, Minna, Nigeria

²Department of Geophysics, School of Physical Sciences, Federal University of Technology, Minna, Nigeria

Email address:

alfaidris207@gmail.com (Alfa Idris Alhaji), a.abbass@futminna.edu.ng (Adetona Abbas Adebayo)

*Corresponding author

To cite this article:

Alfa Idris Alhaji, Salako Kazeem Adeyinka, Rafiu Abdulwaheed Adewuyi, Udensi Emmanuel Emeka, Adetona Abbas Adebayo, Jamilu Shehu. Analysis of Electrical Resistivity Survey Data for Aquifer Potential and Protective Capacity at Mararaba Dan-Daudu Minna, North Central Nigeria. *Hydrology*. Vol. 11, No. 4, 2023, pp. 67-84. doi: 10.11648/j.hyd.20231104.12

Received: September 20, 2023; **Accepted:** October 10, 2023; **Published:** October 28, 2023

Abstract: It is a fact that basement complex regions lacks sufficient overburden that can host sustainable water table, water bearing fractured/weathered rocks referred to as aquifers are usually identified via suitable geophysical methods to proffer solution to water challenges within these regions. This current study targets the exploration of groundwater potential within the Mararaba Dan-daudu community, a suburb of Minna metropolis. Electrical resistivity method was employed to delineate aquifer prospects and their protective capacity within the area of study. The data from thirty-six Vertical Electrical Sounding (VES) survey points were acquired and analysed. Survey points were aligned along six profiles (A – F) with six VES points per profile. Interpretation of VES points along profiles was helpful in determining the number of layers and thickness. The analysis revealed mainly three layers comprising of sand and fresh laterite at the first layer, fractured/weathered basement at the second layer and fresh basement at the third layer. Iso-resistivity mapping was also done at various depths (surface, 5 m, 10 m, 15 m, 20 m, 30 m and 40 m) respectively to investigate the lateral variations of resistivity over a horizontal plane. These showcased the electrical conductance sliced at the depths of interest. Thirteen VES points (A1, A5, A6, B1, B3, B6, C6, D6, E6, F1, F2, F4 and F5) were mapped as having good prospective aquifer properties. Longitudinal conductance was computed for the outlined VES points to determine their Aquifer Protective Capacity (APC). The result of (APC) rating for the 13 VES revealed the frequency and percentage of APC ranged as: 2 VES locations (15.4%) have good APC, 8 VES locations (61.5%) have moderate APC and 3 VES location (23.1%) have weak APC. with only 3 VES locations out of 13 VES locations in the study area revealed weak APC, the results proved that the groundwater potential of the study area has moderately good APC.

Keywords: Aquifer, Electrical Resistivity, Fractured Basement, Vertical Electrical Sounding, Groundwater

1. Introduction

Water is an essential commodity to mankind and it could be found everywhere in the earth's ecosystem. However the water, which exists in such abundance on the earth, is subject to season, time, space and circulation [5]. The search for groundwater has become quite intense in human history. This is due to the fact that government is unable to meet the ever-increasing water demand; inhabitants have had to look for

alternative sources such as streams, shallow wells and boreholes. The amount of surface water available for domestic, industrial and agricultural use is insufficient to fulfil the current demand in the world [40, 41]. The search for sustainable, clean and portable water is of vital importance as it aids in the growth of any community [1, 3, 30, 39].

In the historical past, when there is no visible flow of water along the rivers, people used to dig small pits, in the river alluvium, wait and collect the groundwater coming

through seepage and use it for their drinking purposes and for meeting the domestic needs. More than 60 percent of the global population thrives by using only the groundwater resources. Observation shows that groundwater comes from precipitation such as rain, snow, sheet and hail that soak into the ground and become the groundwater responsible for the spring, wells and boreholes [27]. The shallow depth groundwater has been greatly depleted due to over extraction. Groundwater in the form of aquifer is available in different proportions, in various rock types and at various depths, of the earth. In basement terranes where the water table is not easily accessible, exploration of water bearing rocks (aquifers) becomes the alternative to solving water supply challenges [11, 38].

Two tertiary institutions are proposed for the area in which one (Teachers Training Institute) has taken off. Outside the Mararaban Dan-Daudu several isolated settlements are scattered across the vicinity. A major challenge to these communities which could become adverse in future is the availability of clean and potable water for domestic use. It would be essential to have a futuristic approach to this problem.

The study area is the proposed permanent site of new

Niger state college of education, which is expected to accommodate large number of students, teaching and non-teaching staff of the college meaning there may be need for properly harnessed sources of water supply. This study is focused on evaluating the groundwater potential on the area using Resistivity method.

2. Location and Geology of the Study Area

The study area Mararaba Dan-Daudu, is strategically/geographically located at an inter section between the road that traverse from Kuta – Gwada – Dandaudu - Kafin Koro – Kwakuti – Abuja and that from Minna Dan-Daudu – Sarkin Pawa to Kaduna. It is a town strategically located for future development, hence most of these towns host markets for foods stuff to the Southern part of the country. It is approximately on longitude 6°49' 44.4" E and 6°50' 37.50" E and latitude 9°42' N and 9°42' 49.25" N (Figure 1). Within the area are located two other communities that will benefit from the outcome of this research.

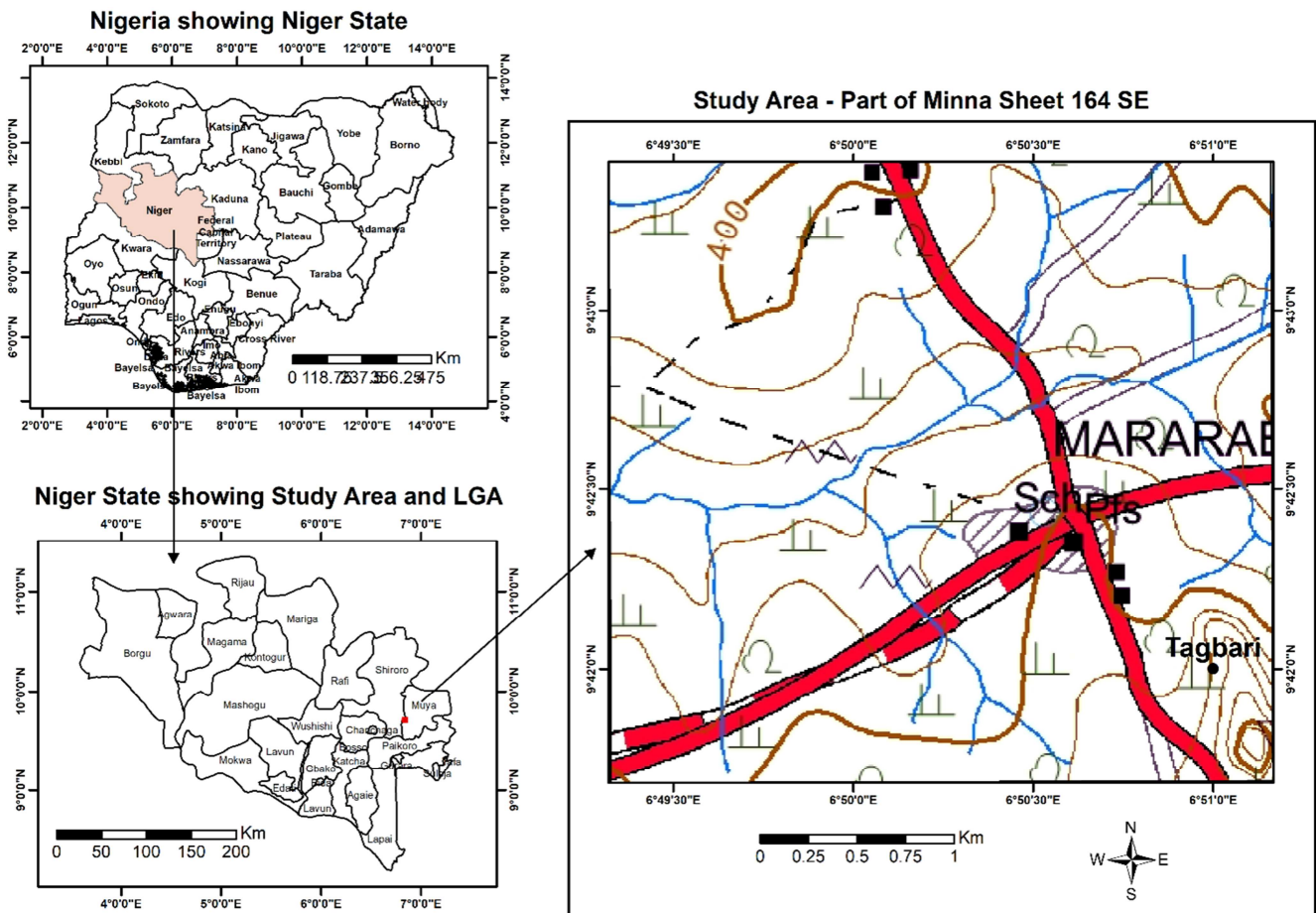


Figure 1. Location map of part of Niger state indicating showcasing study area.

The study area lies within the Basement Complex of Northern Nigeria. The Basement Complex includes all rocks

older than the late proterozoic, [19] and is composed mainly of gneisses, granites, migmatite and some extensive area of

schist, phyllites and Quartzites [29].

This area forms part of Minna granitic formation which consist of meta-sediments and meta-volcanics. These meta-sediments include quartzite, gneisses and the meta-volcanics are granites. Around the northern and central part of this area, the rock types are mainly granites while in the eastern and southern part of the area, cobbles of quartzite are found. Although we can also find pegmatite and quartz vein.

The rock type in this area is made of monolithic rocks of granite origin and it can be grouped into two. The groups are (i) the porphyritic to coarse grained granites and (ii) medium to fine grained granites due to their relative grain size. The rocks are mostly weathered and believed to be part of the older granite suite and are mostly exposed along the river channel.

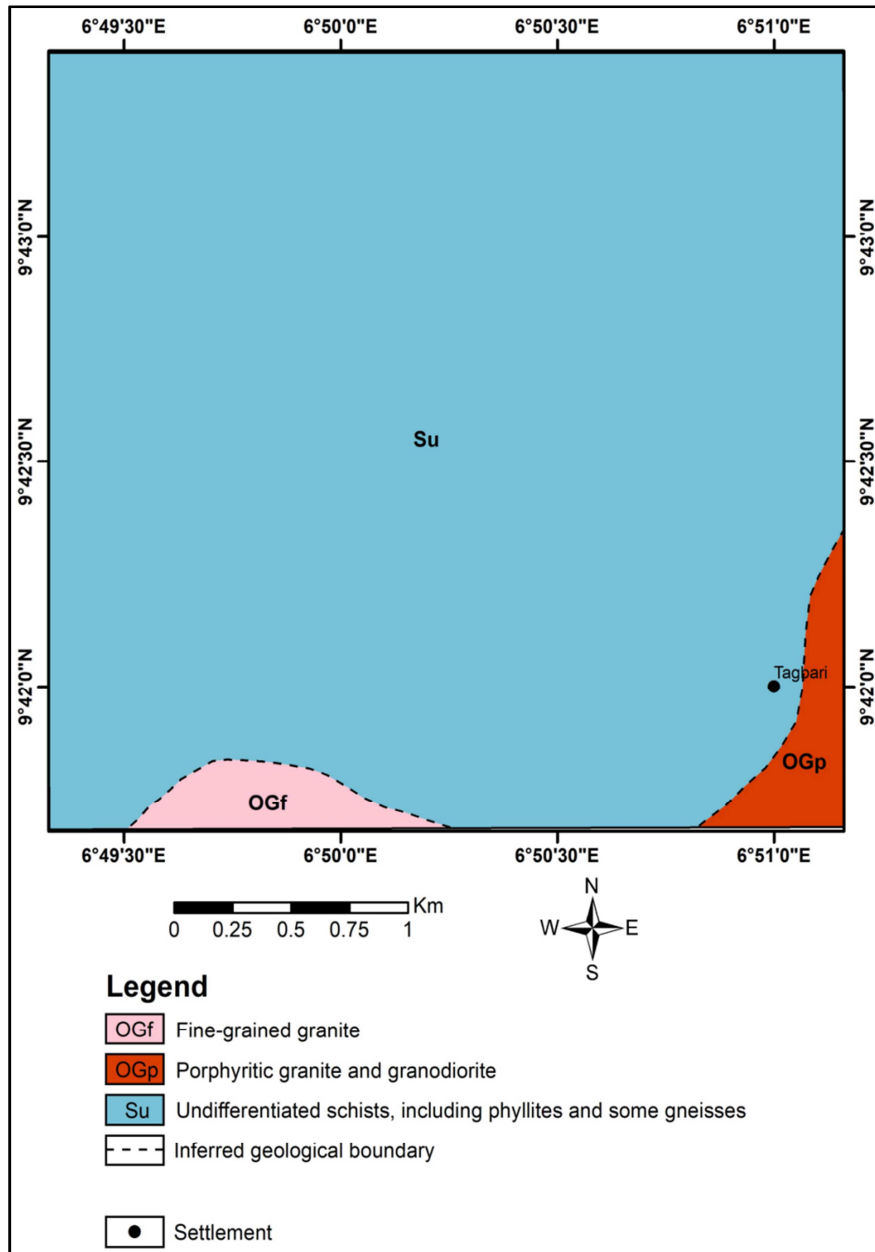


Figure 2. Geological map of Niger state basement complex and sedimentary basin.

Porphyritic to coarse grained granite: this granite is referred to as grained granite due to its size and flat lying. They are mostly exposed along the river channels. They range in sizes between few meters to about 80 m. They are most part cut-crossed by the north-south trending quartz and aplitic veins ranging in length 2 m – 15 m. The rocks usually laid in different direction by joints and few most sinistral and

dextral faults. Sometimes the outcrops are broken and they are characterised by weathering.

Medium to fine grained granite: the rocks are usually flat lying outcrop exposed along the river channels with a relatively elongated outcrops at the surface. They are less weathered when compared to the ones on the north-south part. They are traverse by east-west trending vein and joints. The

rocks are broken boulders in some parts which shows weathering in form of color change and loose rock fragments [6].

3. Materials and Methods

3.1. Materials

- 1) *Terrameter*: This is the major instrument used for Electrical Resistivity Survey. The Terrameters used for the data collection were ABEM SAS 4000 and 1000 series.
- 2) *Electrodes*: These are steel rods of about 30 cm with a base and a pointed end. The pointed end was used to penetrate the ground. Four electrodes were used; the first pair is the potential electrode while the second pair is the current electrode. Their basic function is to pass current into the ground and measure potential between two points.
- 3) *Cables*: The cables were connected to the terrameter on one end and the other was connected to the electrodes.
- 4) *Clips*: Used for connecting cables to electrodes. The clips ensure good electrical contact.
- 5) *Hammer and Cutlass*: Hammer was used to drive the electrodes into the ground.
- 6) *Tapes*: They were used for marking length to be measured on the field as they have been calibrated in meter (m).
- 7) *Global Positioning System and Compass-Clinometer*: These were used for taking coordinates and bearing.

3.2. The Theory of Electrical Resistivity Method

This method involves the passage of artificially generated electric current into the earth through the electrodes and in turn causes variation in the subsurface resistivity. This alters the current flow within the earth and also the distribution of electrical potential. The degree of the effect on electric potential is dependent on the size, shape, location and conductivity of the material within the ground. The measurement of electrical potential and current on the earth's surface makes it possible to obtain information about the resistivity variation of the subsurface in the area of interest [36].

The fundamental equation for resistivity survey is derived from Ohm's law [16, 14, 18]:

$$\rho = \frac{RA}{L} \quad (1)$$

where ρ is resistivity, R is resistance, L is length of homogenous conducting cylinder and A is cross sectional area. Water in the soil's pore spaces and the rock's fractures increases the conductivity of the solid earth, which is primarily made of silicates and is therefore essentially a non-conductor. This turns the rock into a semi-conductor when an electrical current is passed through it. Since the earth is not like a straight wire and it is anisotropic, then equation (1) is thus customized to:

$$\rho = \frac{\Delta V}{I} \cdot 2\pi r \quad (2)$$

where ΔV is change in voltage and r is the radius of current electrode's small hemisphere.

Since the earth is not homogeneous, equation (2) is used to define an apparent resistivity ρ_a which is the resistivity the earth would have if it were homogeneous [16]:

$$\rho_a = \frac{\Delta V}{I} \cdot 2\pi r \quad (3)$$

where $2\pi r$ is then defined as a geometrical factor (G) fixed for a given electrode configuration. The Schlumberger configuration was used in this work. The geometric factor G is thus given as:

$$G = \pi \frac{\left[\left(\frac{AB}{2}\right)^2 - \left(\frac{MN}{2}\right)^2\right]}{2\left(\frac{MN}{2}\right)} \quad (4)$$

where AB is (current electrode spacing) and MN is (spacing between potential electrodes).

Schlumberger spread was utilized for the purpose of depth probing, since the potential electrodes are relatively fixed, while the current electrode spacing is expanded symmetrically about the centre of the spread. Schlumberger is less sensitive to undetected lateral variation in resistivity because the potential difference measured between two points is about one third of the electrode spacing. This electrode effect comes to play due to perturbations caused by the passage of potential electrodes over a superficial in homogeneity which is much greater than those due to current electrodes [28, 45]. Since the movement of the potential electrodes are minimised, the electrode movement effect is also minimized thereby enhancing accuracy of measurement.

3.3. Aquifer Protective Capacity (APC)

Aquifer Protective Capacity (APC) simply means the ability of the overburden unit to retard and filter penetrating ground polluting fluid into the aquiferous unit. According to [2, 22], the protective capacity of an aquifer is compared directly with the sum of the longitudinal conductance of all the layers above the aquifer. The protective capacities of identified aquifers in the study area were determined from the longitudinal conductance of the geoelectric layers above the aquifer. This evaluation creates awareness on the state of the aquifers' possibilities to contamination regarding to human activities and industrial discharge [26]. Therefore, the study considered it essential to evaluate the protective capacity of the saturated zone in each location. Aquifer protective capacity, estimates the vulnerability of the underlying aquifer to contamination.

The longitudinal conductance of the overburden layer was obtained using [43] formula:

$$S = \sum_{i=1}^n \frac{h_i}{\rho_i} \quad (5)$$

where h = the saturated thickness of each layer

ρ - The layer resistivity

i = Number of layers
 S = Longitudinal conductance.

Table 1. Longitudinal Conductance/Protective Capacity Rating. Modified after [43, 21].

Longitudinal conductance (mho)	protective capacity rating
>10	excellent
5-10	very good
0.7-4.9	good
0.2-0.69	moderate
0.1-0.19	weak
Below 0.1	poor

4. Analysis and Interpretation of (VES)

The apparent resistivity in ohm-metre determined from the data collected from the thirty-six (36) VES were further analysed as follows:

- 1) Plotting of resistivity-depth (AB/2) curves for the thirty-six (36) VES points using WinResist version 1.0, (2004) software package for automatic interpretation of Schlumberger sounding.
- 2) The number of layers, thickness, depth where a layer is starting from and average resistivity values were determined from the resistivity-depth curves.
- 3) The information determined were summarised in tabular form. (Tables 3, 4; Appendix: Table A1-A4).
- 4) Geologic sections with their average resistivity values were produced along the profiles using range of resistivity values for various rocks in basement complex (Table 2) compiled by [37, 4, 12] as cited by [13].

Table 2. Range of Resistivity values for various rock types in Basement complex used in deriving the geologic sections [44].

Rock type	Range of resistivity (Ωm)
Fadama loam	30-90
Weathered laterite	150-900
Fresh laterite	900-3500
Granite	300-10 ⁵
Clays	1-100

Rock type	Range of resistivity (Ωm)
Gravel	100-1500
Alluvium and sand	10-800
Quartzite (various)	10 -2 × 10 ⁸
Weathered laterite	150 – 900
Weathered basement	20 - 500
Fractured basement	500 - 1000
Fresh basement	>1000

4.1. Summary of the VES Results Analysis Along Profile A

General summary of the VES analysis along profile A is as shown in Table 3. There are six (6) VES points on the profile. All the six points have three layers with H curve-type, that is $\rho_1 > \rho_2 < \rho_3$.

The resistivity values for the whole profile ranges from 36.1 Ωm to 4064.3 Ωm . The resistivity values on the first layer ranges from 157.4 Ωm to 3943.8 Ωm and the thickness range between 0.6 m to 3.6 m, the maximum resistivity value on the first layer is at VES station A₆ (3943.8 Ωm) (Fresh Laterite) which is towards the eastern part of the surveyed area, where an outcrop was observed in the field, while minimum value is at VES station A₃ (157.4 Ωm , weathered laterite, Table 2). The resistivity of the second layer range from (36.1 Ωm) A₂ to (89.7 Ωm) A₆ (fadama loam and clay) and the corresponding thickness range between 8.2 m to 33.4 m, the thickest VES point is at A₅ and thinnest is at VES A₄. The low apparent resistivity of second layer maybe due to aquifer presence, especially at VES points A₅ and A₆, where the layer thickness are high. The third layer has resistivity value range from 679.1 Ωm (A₁) to 4064.3 Ωm (A₃). Profile A₆ has the highest first layer apparent resistivity (3943.8 Ωm) while the highest basement apparent resistivity (4064.3 Ωm), was observed at VES A₃. The depth of occurrence of basement along profile A, range from 9.6 m to 33.7 m. VES A₄ has shallowest basement starting from 9.6 m while VES A₅ has the thickest basement starting from 33.7 m and all end at infinity. Except at VES A₁, where basement apparent resistivity value is that of weathered/Fractured layer (679.1 Ωm), the rest resistivity of the third/basement layer are of fresh basement (Table 3).

Table 3. Summary of VES results analysis along profile A.

VES point	Type of curve	No of layers	Average resistivity (Ωm)	Layer thickness (m)	Depth starting from (m)
A ₁	H	1	1541.6	3.6	0.0
		2	41.2	13.3	3.6
		3	679.1	∞	16.9
A ₂	H	1	648.0	1.4	0.0
		2	36.1	9.1	1.4
		3	2555.7	∞	10.5
A ₃	H	1	157.4	0.6	0.0
		2	38.0	13.9	0.6
		3	4064.3	∞	26.8
A ₄	Ha	1	331.4	1.4	0.0
		2	72.5	8.2	1.4
		3	1196.0	∞	9.6
A ₅	H	1	976.7	1.3	0.0
		2	42.0	33.4	1.3
		3	3018.7	∞	34.7
A ₆	H	1	3943.8	1.6	0.0
		2	89.7	20.5	1.6
		3	931.2	∞	22.1

4.2. Summary of the VES Results Analysis Along Profile F

There are six (6) VES points on profile F as shown in Table 4 and three distinct layers are prominent on all the VES points, with H curve-Type.

The first layer has a resistivity values range between 66.2 Ωm (alluvium and sand) and 2266.6 Ωm (fresh laterite) and the corresponding thickness is between 0.6 m and 3.8 m. The

maximum thickness on the first layer is at VES F₂ (3.8 m) and the minimum thickness is at VES F₂ (0.6 m). The resistivity value of the second layer ranges from 15.8 Ωm (Clay) to 421.8 Ωm (Weathered laterite) and the corresponding thickness range between 17.8 m and 44.5 m. The thickest VES point is at F₄ and the thinnest is at VES point F₃.

Table 4. Summary of VES Results Analysis along Profile F.

VES point	Type of curve	No of layers	Average resistivity (Ωm)	Layer thickness (m)	Depth starting from (m)
F ₁	H	1	1039.3	2.5	0.0
		2	80.7	28.7	2.5
		3	4272.9	∞	31.2
F ₂	H	1	1401.3	3.8	0.0
		2	105.5	35.4	3.8
		3	1687.1	∞	39.2
F ₃	H	1	2545.7	1.3	0.0
		2	421.8	17.7	1.3
		3	11725.6	∞	19.0
F ₄	H	1	2266.6	0.6	0.0
		2	172.4	44.5	0.6
		3	882.4	∞	44.5
F ₅	H	1	66.2	1.1	0.0
		2	61	30.1	1.1
		3	1414.4	∞	30.1
F ₆	H	1	194.2	1.2	0.0
		2	15.8	17.8	1.2
		3	7596.8	∞	17.8

The third layer has resistivity range from 882.4 Ωm (weathered/fractured basement) to 7596.8 Ωm (fresh basement) (Table 4), with infinite thickness. The shallowest depth is at VES F₆ (17.8 m) while the deepest depth is at VES F₄ (44.5 m). The first layer resistivity indicated Clay, Weathered lateritic topsoil. Second layer has resistivity values which correspond with that of fadama loam, clay, alluvium and sand, they have very low resistivity values compared with the resistivity values of first and the third layers.

Table of summary for VES result analysis for profile B to E is appended on appendix (Tables A1-A4).

4.3. General Deductions and Correlations of Iso-Resistivity Contour Maps at Various Depths

The analysis from VES result analysis for profiles makes it much easier to draw a certain number of deductions as regarding the depth and thickness of each layer and zone of water saturation known as (aquifer).

Iso-resistivity maps reflect the lateral variations of resistivity over a horizontal plane at a given depth. In other words, these Iso-resistivity contoured maps indicate resistivity distribution in an area against the distance of current electrodes. This was achieved by plotting the resistivity data corresponding to the depth of interest (picked from the log table) for all the study area. Surfer 13 software version was used to contour these maps which showed the conductivity pattern with depth through the horizontal slicing of the study area. The depths of interest are, the surface, 5 m

depth, 10 m depth, 15 m depth, 20 m depth, 30 m depth and 40 m depth. Contour maps for surface, 5 m depth, 10 m depth, 15 m depth, 20 m depth and 30 m depth is presented on appendix (Figure A1-A6).

4.4. Interpretation of Iso-Resistivity Contour Map at 40 m

The Iso-resistivity contour map at 40 m depth was produced as shown in Figure 3, the map was contoured at an interval of 100 Ωm .

The resistivity value ranges from 0 Ωm to 4400 Ωm , the low resistive ($\rho < 600 \Omega\text{m}$) area still occurred at this depth, which indicate that weathered basement still continued at this depth, areas where this occurred that is, the eastern part of the studied area, and the area where the villagers resides. The low resistivity here maybe as a result of human activities going on there, such as refuse dump.

Areas where the resistivity is that of weathered/fractured basement are very few and they are toward western part. Finally, at the western part of the map, is where the resistivity values are that of fresh basement ($\rho > 1000 \Omega\text{m}$). A trailing small point with $\rho < 200 \Omega\text{m}$, that featured at 30 m depth probing, still appeared at the same point at 40 m depth (figure 3); this might be as a result of a conducting mineral at that point, activity of the artisan miners on the studied area also confirmed such, they were notice packing the top sand to go and wash for gold mining. Also, not far from this point, is a very deep hole (more than 16 ft) dug by the artisan miners, for their mining activities.

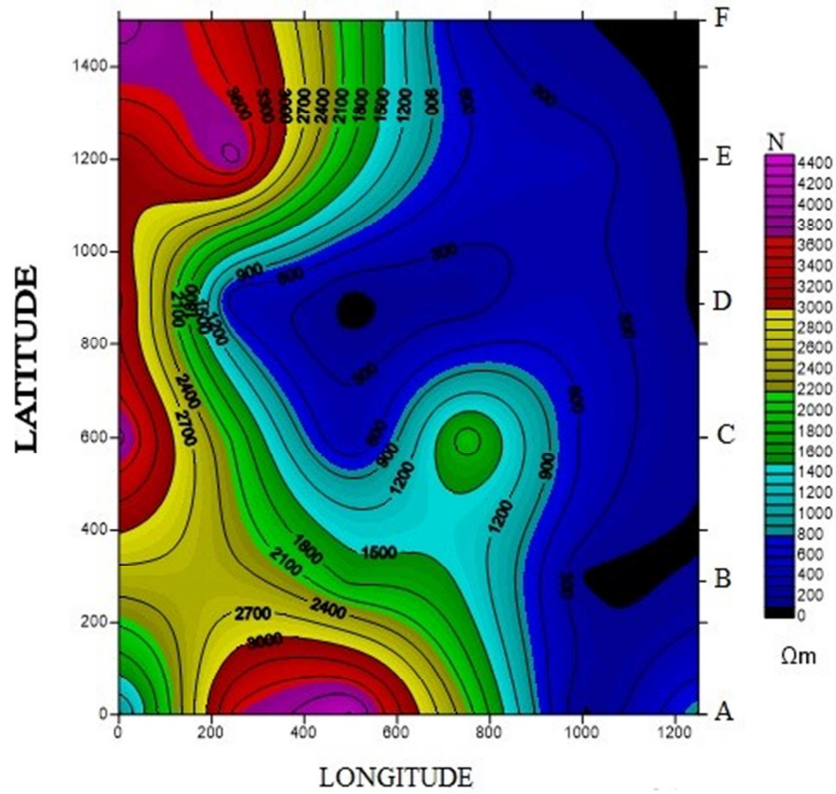


Figure 3. Iso-Resistivity map at 40 metres, Contour Interval = 100 m.

4.5. Interpretation of Iso-Resistivity Contour Map for the Second Layer

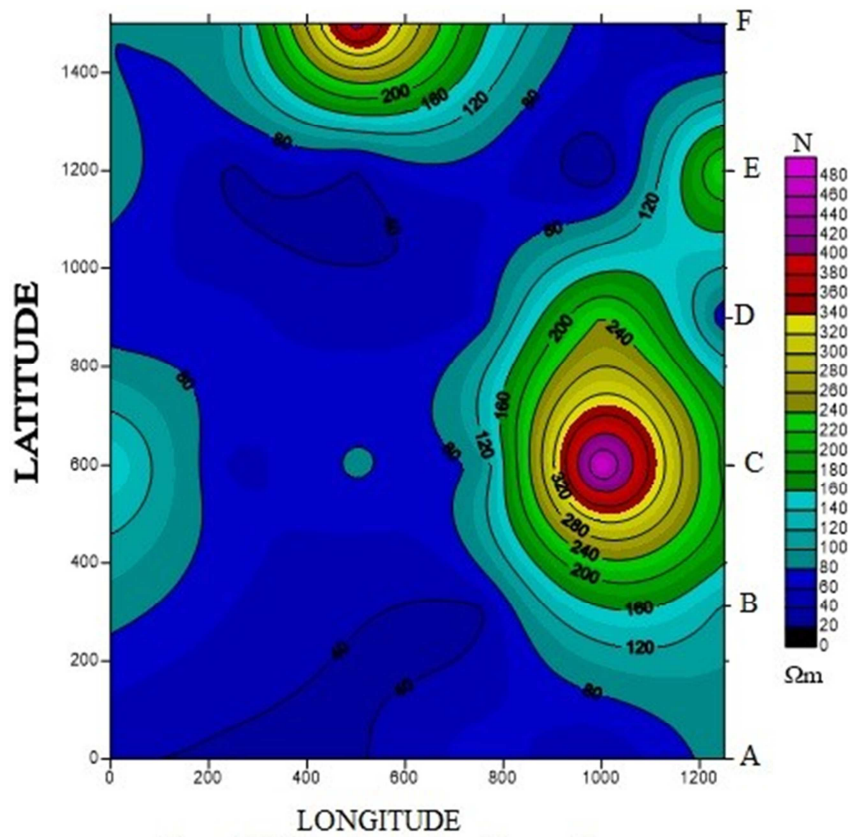


Figure 4. Iso-Resistivity map of Second Layer, Contour Interval = 20 m.

The Iso-resistivity contour map of second layer was produced as shown in Figure 4, the map was contoured at an interval of 20 Ωm , the contour lines trend towards North-Western direction.

The resistivity value ranges from 0 Ωm to 480 Ωm . From the map, it is observed that the resistivity value of the whole area is generally low, this may be due to the presence of water and some conductive mineralisation at this layer. The blue colour with apparent resistivity (ρ) which ranges between 20 and 80 Ωm and dominate the entire map has resistivity value which corresponds to the resistivity of clay (Table 2), The areas with yellow, red and brown colours which appear at North central and East central parts of the study area correspond to that of weathered basement.

Comparing trends at 15 m depth (appendix 1d) and entire second layer (Figure 4), it was noticed that they almost have the same value, even where high resistivity closure was noticed on north central of depth 15 m map, Profile F, VES F₃, it was also noticed at the same VES point on figure 4, this implies that second layer was concentrated within 15 m depth of the surveyed area.

4.6. Interpretation of Iso-Resistivity Contour Map for the Third Layer

The Iso-resistivity contour map of the third layer was produced as shown in Figure 5, the map was contoured at an interval of 100 Ωm , the contour lines looks almost parallel in the North-Southern direction while the closures trend North-Eastern direction.

The resistivity value ranges from 400 Ωm to 4800 Ωm . From the map, it is observed that the resistivity value of the whole area is generally high compared with that of second layer. The whole area has resistivity of either Weathered or Fractured or fresh basement. Blue colours has resistivity value which corresponds to the resistivity of Weathered/fractured basement (Table 2).

Comparing trends at 40 m depth (Figure 3) and third layer (Figure 5), it was observed that their contour lines look alike, (parallel) with high resistivity values, at the western part and low resistivity value at the eastern parts of the two figures, this implies also that, third layer resistivity concentrated at the depth of 40 m.

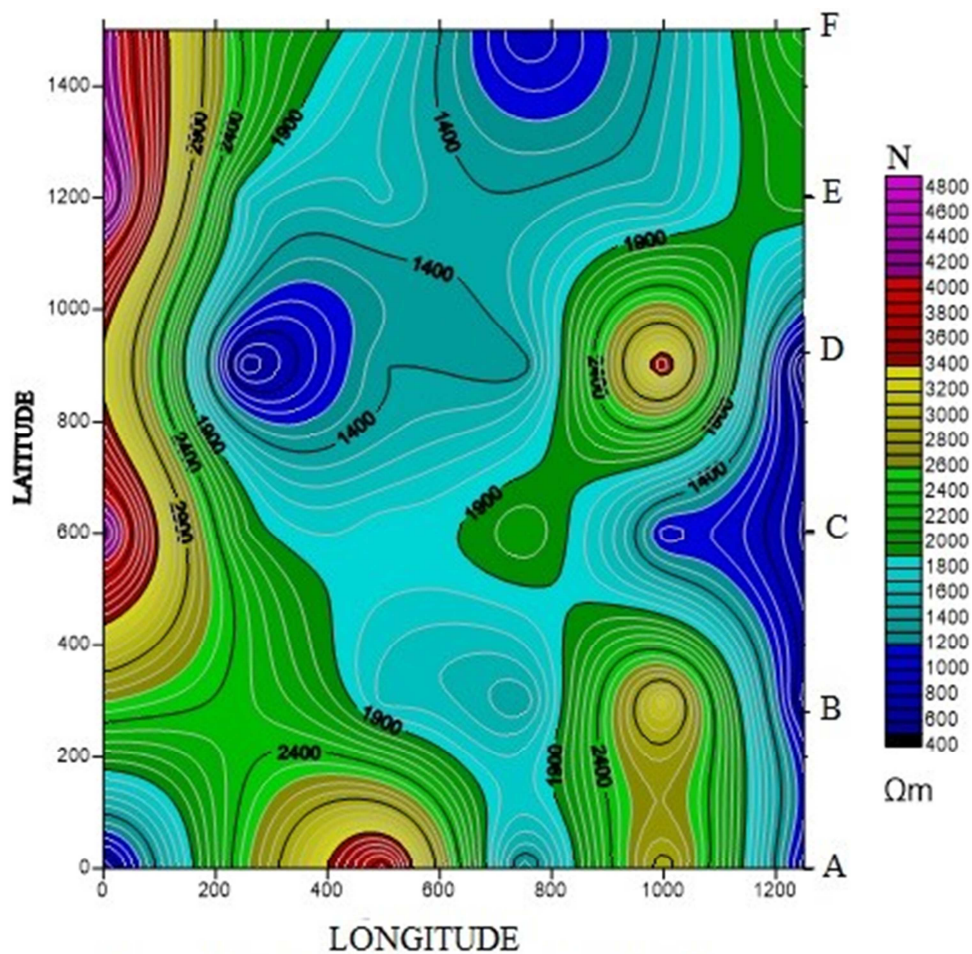


Figure 5. Iso-Resistivity map of Third Layer, Contour Interval = 100 m.

The areas with yellow, red and brown colours which appear at all the Western, South central and North-Eastern parts of the study area correspond to that of Fresh basement.

4.7. Interpretation of Contour Map for the Overburden Thickness

Figure 6 is the contour map of the depth to the basement or overburden thickness map, the map was contoured at an interval of 5 m.

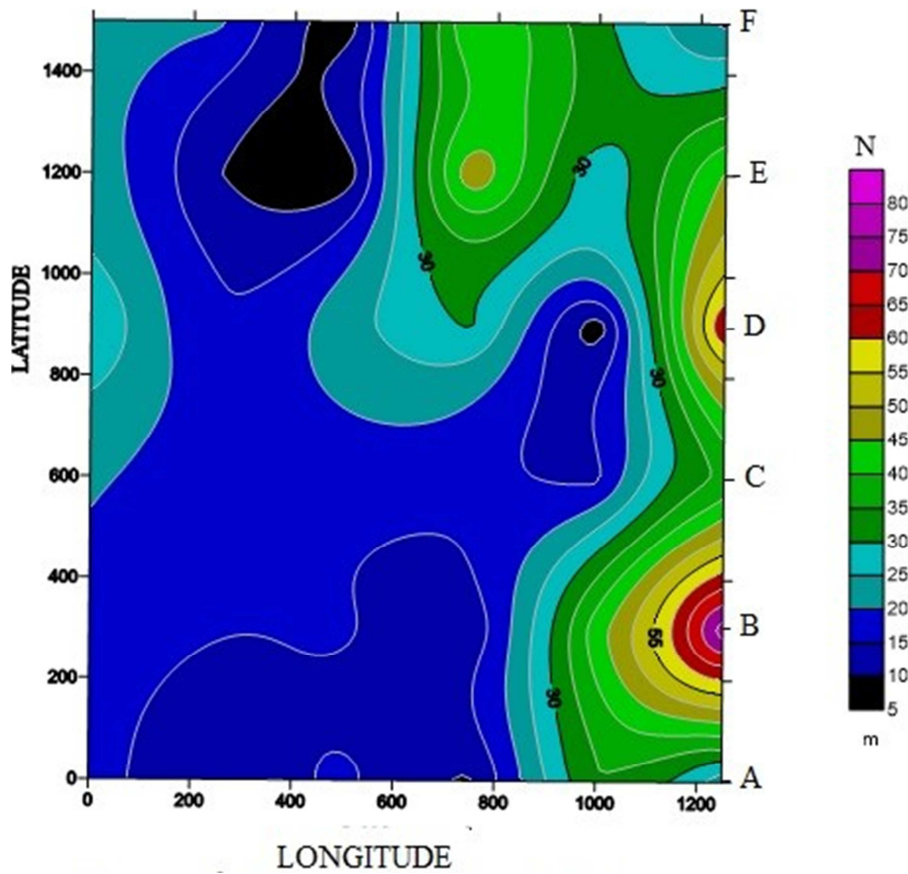


Figure 6. Contour map of Overburden Thickness, Contour Interval = 5 m.

The depth ranges from 5 m to 85 m, the depth to basement values used for the contour map corresponds to the depth to the last layer for the whole VES points in the surveyed area. From the map, it was observed that the deepest area was found around the eastern part, Profile B, VES B₆ and Profile

D, VES D₆) and the shallowest area is found at Profile E, VES E₅, this may be attributed to the very deep channel washed away by gully erosion found around that area, which might had washed away the top soil around that point.

Table 5. Depth to Fresh Basement of the Area, Longitudinal Conductance, Protective Capacity Rating and Curve Type.

VES Station	Elevation (m)	Depth To Basement (m)	Longitudinal Conductance (mho)	Protective Capacity Rating	Curve Type
A ₁	397	16.9	0.40	Moderate	H
A ₂	387	10.5	0.29	Moderate	H
A ₃	393	26.8	0.71	Good	H
A ₄	358	9.6	0.13	Weak	H
A ₅	397	34.7	0.80	Good	H
A ₆	406	22.1	0.25	Moderate	H
B ₁	375	40.1	0.45	Moderate	H
B ₂	378	10.1	0.19	Weak	H
B ₃	388	39.4	0.10	Weak	H
B ₄	408	73.6	0.63	Moderate	H
C ₁	389	20.9	0.13	Weak	H
C ₂	377	10.1	0.18	Weak	H
C ₃	390	17.2	0.20	Moderate	H
C ₄	396	14.8	0.11	Weak	H
C ₅	391	14.3	0.03	Poor	H
C ₆	379	35.9	0.19	Weak	H
D ₁	379	21.2	0.33	Moderate	H
D ₂	387	15.3	0.22	Moderate	H

VES Station	Elevation (m)	Depth To Basement (m)	Longitudinal Conductance (mho)	Protective Capacity Rating	Curve Type
D ₃	405	23.6	0.04	Poor	H
D ₄	405	12.2	0.20	Moderate	H
D ₅	388	41.2	0.17	Weak	H
D ₆	401	65.6	0.11	Weak	H
E ₁	379	28.7	0.29	Moderate	H
E ₂	382	10.5	0.29	Moderate	H
E ₃	381	6.7	0.17	Weak	H
E ₄	384	12.4	0.18	Weak	H
E ₅	383	5.5	0.30	Moderate	H
E ₆	386	45.5	0.19	Weak	H
F ₁	389	31.2	0.39	Moderate	H
F ₂	390	39.2	0.37	Moderate	H
F ₃	383	19.0	0.05	Poor	H
F ₄	384	44.5	0.26	Moderate	H
F ₅	383	30.1	0.49	Moderate	H
F ₆	379	17.8	1.13	Good	H

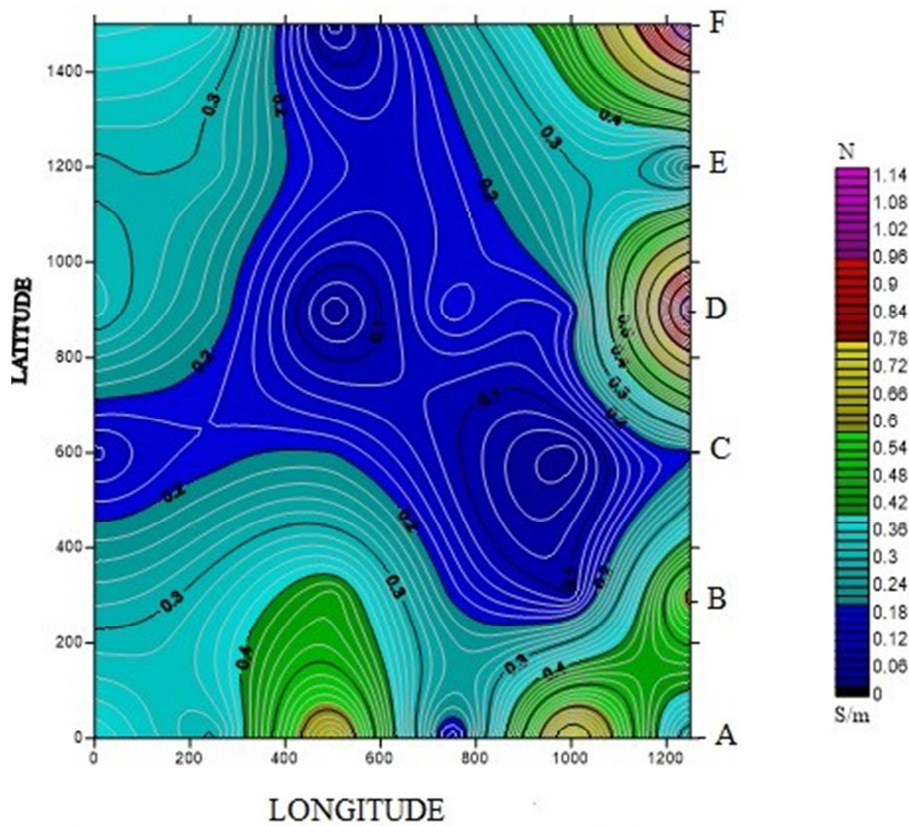


Figure 7. Contour map of Longitudinal Conductance, Contour Interval = 0.02 S/m.

From Table 5, it could be seen that the aquifer potentials have poor, weak, moderate and good protective capacities, having a longitudinal conductance ranging from 0.03 mho to 1.13 mho. The longitudinal conductance was calculated using equation 5. The highest longitudinal conductance for the aquifer potential was seen at VES F₆ (1.13) and the lowest was seen at VES C₅ (0.03).

The contour map of longitudinal conductance for the whole study was produce as shown in Figure 7, the map was produced at an interval of 0.02 mho.

The longitudinal conductance ranges from 0 mho to 1.14 mho, with the highest at VES F₆, while the lowest is at VES C₅.

4.8. Aquifer Protective Capacities Evaluation

In a basement complex terrain, areas with overburden thickness of 15 m and above and fractured layer resistivity of 400 Ωm are good for groundwater development [8]. In addition, in basement complex, the areas with low resistivity, thick overburden and fractured bedrock constitute the aquifer units [25, 33, 34]. The author [7, 23] stated that the highest groundwater yield in basement complex is often obtained from a fractured aquifer or a subsurface sequence that has a combination of a significantly thick and sandy weathered layer. In view of above, 13 VES points were delineated as aquifer potentials of the surveyed area, they are as shown in

Table 6.

Table 6. Aquifer Potential for the Study Area.

VES Point	Latitude	Longitude	Fractured/Fresh basement Resistivity (Ωm)	Layer Depth Starting From (m)	Longitudinal Conductance (Ohm^{-1})	Protective Capacity Rating
A ₁	1073000	262100	679.1	16.9	0.40	Moderate
A ₅	1073000	263100	3018.7	34.7	0.80	Good
A ₆	1073000	263350	931.2	22.1	0.25	Moderate
B ₁	1073300	262100	1653.9	40.1	0.45	Moderate
B ₃	1073300	262350	3304.4	39.4	0.10	Weak
B ₆	1073300	263350	748.3	73.6	0.63	Moderate
C ₆	1073600	263350	676.3	35.9	0.19	Weak
D ₆	1073900	263350	502.5	65.6	1.11	Good
E ₆	1074200	263150	911.1	45.5	0.19	Weak
F ₁	1074500	261900	4272.9	31.2	0.39	Moderate
F ₂	1074500	262150	1687.1	39.2	0.37	Moderate
F ₄	1074500	262650	882.4	44.5	0.26	Moderate
F ₅	1074500	262900	1414.4	30.1	0.49	Moderate

From Table 6, it is shown that the aquifer potentials have weak, moderate and good protective capacities having a longitudinal conductance ranging from 0.10 Ohm^{-1} to 1.11 Ohm^{-1} . The highest longitudinal conductance for the aquifer potential was seen at VES D₆ (1.11 Ohm^{-1}) and the lowest was seen at VES B₃ (0.10 Ohm^{-1}).

According to the aquifer protective capacity (APC) rating of [43, 21], the frequency and percentage of APC are ranged as follows; 2 VES locations (15.4%) have good APC, 8 VES locations (61.5%) have moderate APC and 3 VES location (23.1%) have weak APC (Table 6). These show that only 3 VES locations out of 13 VES locations in the study area revealed weak APC (Figure 7). The impermeable and thick clay overburden materials which are characterized by low hydraulic conductance serve as natural filters to any percolating fluid [31, 42, 15]. These material reduce the rate of movement of the fluid through them hence, increasing their residence time and offering better protection to the underlying aquifers [17].

An effective groundwater protection is provided by protective layers with sufficient thickness and low hydraulic conductivity leading to high rate of percolating water [20]. Areas with high longitudinal conductance (thick overburden and low resistivity) constitute regions of excellent – good aquifer protective capacity in which such locations have sufficient seal from groundwater contamination. Locations with moderate aquifer protective capacity are less susceptible or rare to contamination while areas with weak – poor APC are susceptible to contamination [10]. These results show that the groundwater potential of the study area is moderately good and indefinite locations of weak aquifer protective capacity of the overburden.

In a basement complex terrain, areas with fresh basement layer depth of 4 m and below are good for civil engineering work. [8, 32, 35], stated that, where the overburden layer thickness is thick, such an area is unsuitable for construction of high-rise buildings but very good area for groundwater exploration. They also stated that incompetent zone for erecting of high-rise structures, are zones (shallow/deep fracture) but are better sites for hydrogeological purposes.

And the competent zones are the poorly weathered zones which are better sites for erecting of heavy structures.

5. Conclusion

For this research work, Electrical Resistivity data were collected using Vertical Electrical Sounding (VES) using Schlumberger array across all the thirty six (36) VES points, taken along the 6 profiles. This Schlumberger electrode layout was used, because the smaller separation of the potential electrodes reduces noise due to ground current (from cultural and telluric sources) which may limit the useful depth of penetration. Similarly, the maximum current electrode separation of 430 m and potential electrode of 100 m were reached and this corresponds to 215 m probed depth (i.e AB/2), there was no need for data reduction or repeated measurement since the receiver of SAS 4000 discriminates noise and measures voltages corrected with transmitted signal current. The system has the built-in function to average the best measurement of maximum of four staking with the standard deviation of unity or even less [45]. The apparent resistivity data were generated from resistance values, using equation (3) and (4). WIN-resist software was used to interpret the data. This particular software perform automatic interpretation of the Schlumberger sounding curves which then gives the equivalent numbers of n-layer model input from the apparent resistivity data of particular sounding point, which then converts the apparent resistivity as a function of electrode spacing the true resistivity value as a function of depth. The vertical electrical sounding data were interpreted to obtain geo-electric section, geologic section and finally iso-resistivity maps at various depths.

The result obtained show that the area is generally underlain by three geologic formation (lateritic top soil, weathered/fracture basement and fresh basement. With average first layer resistivity of $1065.6 \text{ }\Omega\text{m}$, with highest value of $3943.8 \text{ }\Omega\text{m}$ at VES A₆ and lowest value of $1331.6 \text{ }\Omega\text{m}$ at VES D₄, the layer also has an average thickness of 1.7 m with highest value of 4.0 m (VES B₄) and lowest value of 0.6 m (VES A₃ & F₄). Second layer has average resistivity

value of 129.5 Ωm with highest value of 556 (D_3) and lowest value of 15.8 Ωm (F_6) with corresponding average thickness of 23.0 m which ranges from 4.1 m VES E_5 to 73.6 m VES B_4 . Finally third layer has an average resistivity of 3573.3 Ωm , with least value of 776.3 Ωm and highest value of 22750.7 Ωm with depth averagely starting from 25.6 m, the least depth starting from 5.5 E_5 and deepest value starting from 73.6 m (E_5).

With regard to aquifer protection capacity (APC), only 3 VES locations out of 13 VES locations in the study area that was delineated as aquifer potential, has weak APC (Table 6), (Figure 7). The results proved that the groundwater potential of the study area has moderately good APC; hence the aquifers of the study area constitute definite overburden thickness with clay which serves as natural filter to percolating fluids. The result also showed that the aquifers in the study area have moderate-low vulnerability to contamination because the APC is moderately good, except for only 3 VES points, which have weak APC.

The presence of interconnectivity of fracture zones in the study area showed that the area has good prospects for groundwater development and it can be recommended that the search for groundwater in the study area should be aimed at searching for fractured zones where overburden is relatively thin. Areas that are extensively fractured and where the fractures are deep are considered as weak zones and considered suitable zones for groundwater development [7, 32].

VES analysis revealed three lithologic sequences which include topsoil, weathered layer and fractured or fresh bedrock. H-type are the curve types obtained from the VES data with overburden thickness ranging from 8.2 m to 73.6 m. The bed rock is averagely covered with thick overburden which is unsuitable for construction of heavy structures but would be useful for small scale groundwater exploration [33, 34, 35] such as development of hand-dug well and hand-pump well. The iso-resistivity map of the weathered layer revealed the area is of good groundwater potential but incompetent for engineering structures.

Appendix

Tables A1-A4: Summary of VES results analysis along profile B, C, D and E.

Table A1. Summary of VES results analysis along profile B.

VES point	Type of curve	No of layers	Average resistivity (Ωm)	Layer thickness (m)	Depth starting from (m)
B ₁	H	1	209.8	2.1	0.0
		2	42.2	13.6	2.1
		3	1653.9	∞	40.1
B ₂	H	1	1564.0	1.3	0.0
		2	52.4	10.1	1.3
		3	1395.8	∞	10.1
B ₃	H	1	724	3.3	0.0
		2	395.6	39.4	3.3
		3	3304.4	∞	39.4
B ₄	H	1	436.7	4.0	0.0
		2	117.5	73.6	4.0
		3	748.3	∞	73.6

Table A2. Summary of VES results analysis along profile C.

VES point	Type of curve	No of layers	Average resistivity (Ωm)	Layer thickness (m)	Depth starting from (m)
C ₁	H	1	2126.0	1.5	0.0
		2	158.6	19.4	1.5
		3	4483.8	∞	20.9
C ₂	H	1	210.2	0.7	0.0
		2	54.7	9.4	0.7
		3	5008.6	∞	10.1
C ₃	H	1	1961.7	1.0	0.0
		2	85.7	16.2	1.0
		3	1892.0	∞	17.2
C ₄	H	1	1221.7	1.2	0.0
		2	86.7	13.6	1.2
		3	22750.7	∞	14.8
C ₅	H	1	1227.3	1.4	0.0
		2	484.2	12.9	1.4
		3	1033.1	∞	14.3
C ₆	H	1	775.2	0.9	0.0
		2	190.6	35.0	0.9
		3	676.3	∞	35.9

Table A3. Summary of VES Results Analysis along Profile D.

VES point	Type of curve	No of layers	Average resistivity (Ω m)	Layer thickness (m)	Depth starting from (m)
D ₁	H	1	298.4	1.7	0.0
		2	63.9	19.5	1.7
		3	12663.2	∞	21.2
D ₂	H	1	571.1	1.3	0.0
		2	68.1	14.0	1.3
		3	598.1	∞	15.3
D ₃	H	1	749.2	2.4	0.0
		2	556.0	21.2	2.4
		3	1398.9	∞	23.6
4 _b	H	1	1853.5	0.9	0.0
		2	62.2	11.3	0.9
		3	1545.1	∞	12.2
D ₅	H	1	1210.0	1.8	0.0
		2	242.0	39.4	1.8
		3	8405.0	∞	41.2
D ₆	H	1	1804.3	2.3	0.0
		2	59.3	63.3	2.3
		3	502.5	∞	65.6

Table A4. Summary of VES Results Analysis along Profile E.

VES point	Type of curve	No of layers	Average resistivity (Ω m)	Layer thickness (m)	Depth starting from (m)
E ₁	H	1	414.7	2.6	0.0
		2	98.6	26.1	2.6
		3	5372.8	∞	28.7
E ₂	H	1	888.9	3.5	0.0
		2	36.0	7.0	3.5
		3	3998.2	∞	10.5
E ₃	H	1	147.5	0.7	0.0
		2	39.5	6.0	0.7
		3	1625.8	∞	6.7
E ₄	H	1	426.2	1.1	0.0
		2	69.2	11.3	1.1
		3	687.6	∞	12.4
E ₅	H	1	966.9	1.4	0.0
		2	18.4	4.1	1.4
		3	813.7	∞	5.5
E ₆	H	1	1331.6	1.5	0.0
		2	244.9	44.0	1.5
		3	911.1	∞	45.5

Figures A1-A6: Iso-Resistivity maps for surface, 5 m, 10 m, 15 m, 20 m and 30 m.

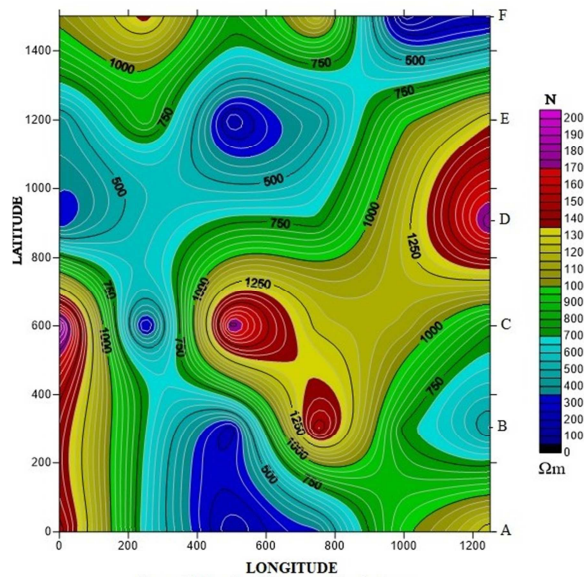


Figure A1. Iso-Resistivity maps for surface.

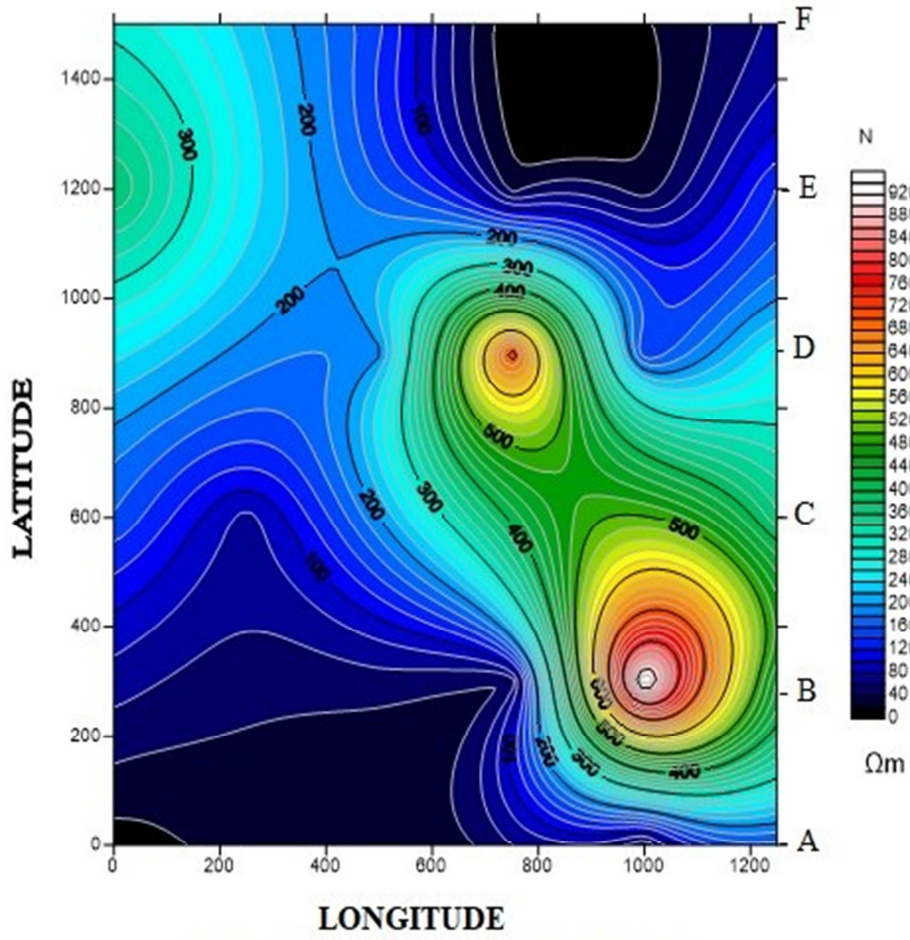


Figure A2. Iso-Resistivity maps for 5 m depth.

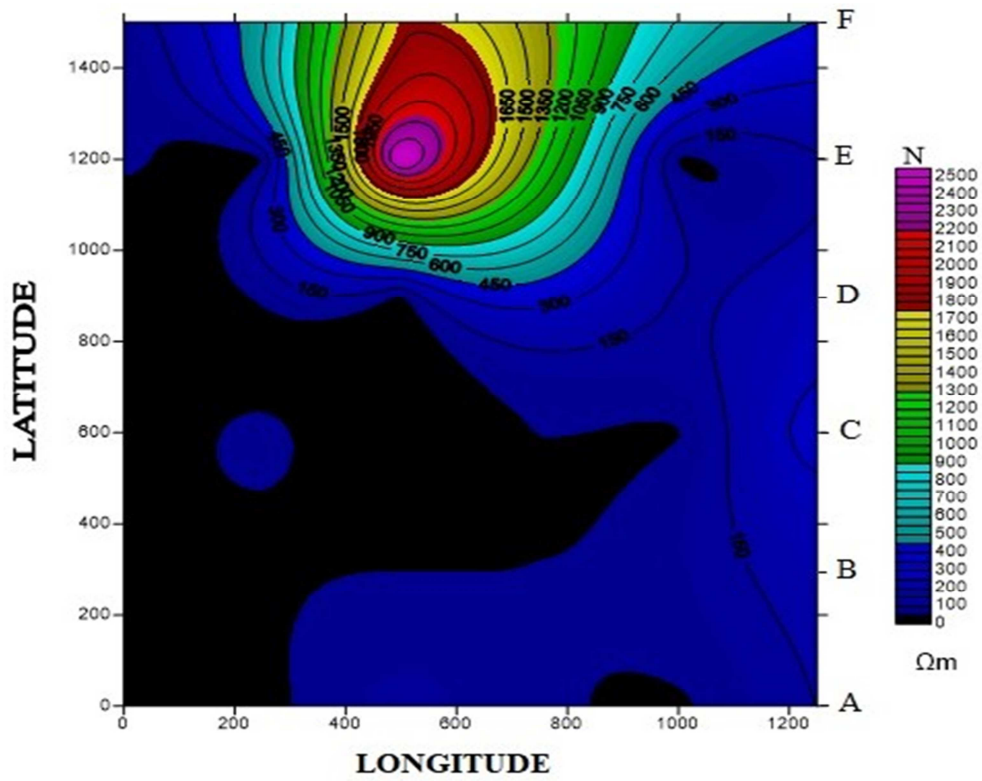


Figure A3. Iso-Resistivity maps for 10 m depth.

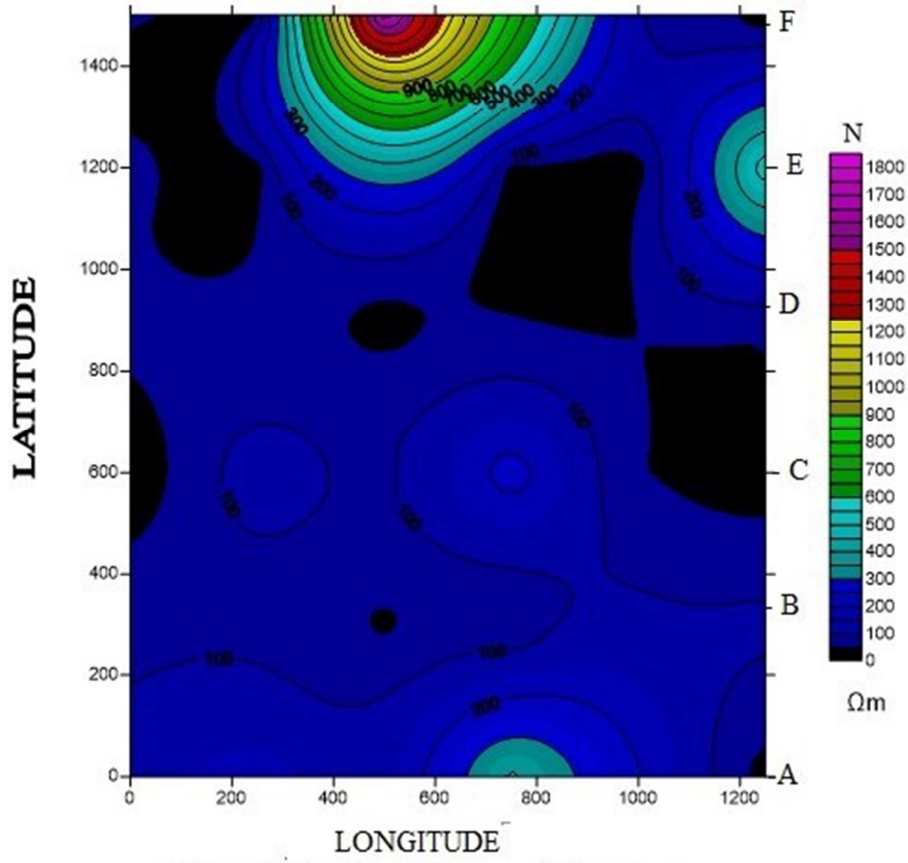


Figure A4. Iso-Resistivity maps for 15 m depth.

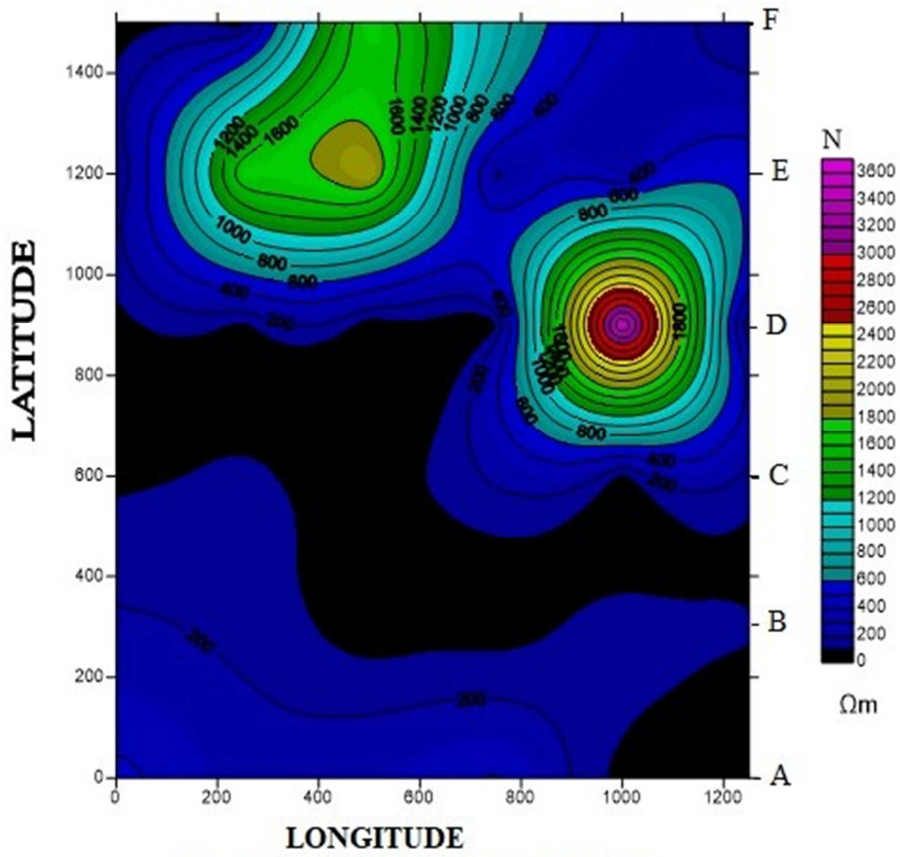


Figure A5. Iso-Resistivity maps for 20 m depth.

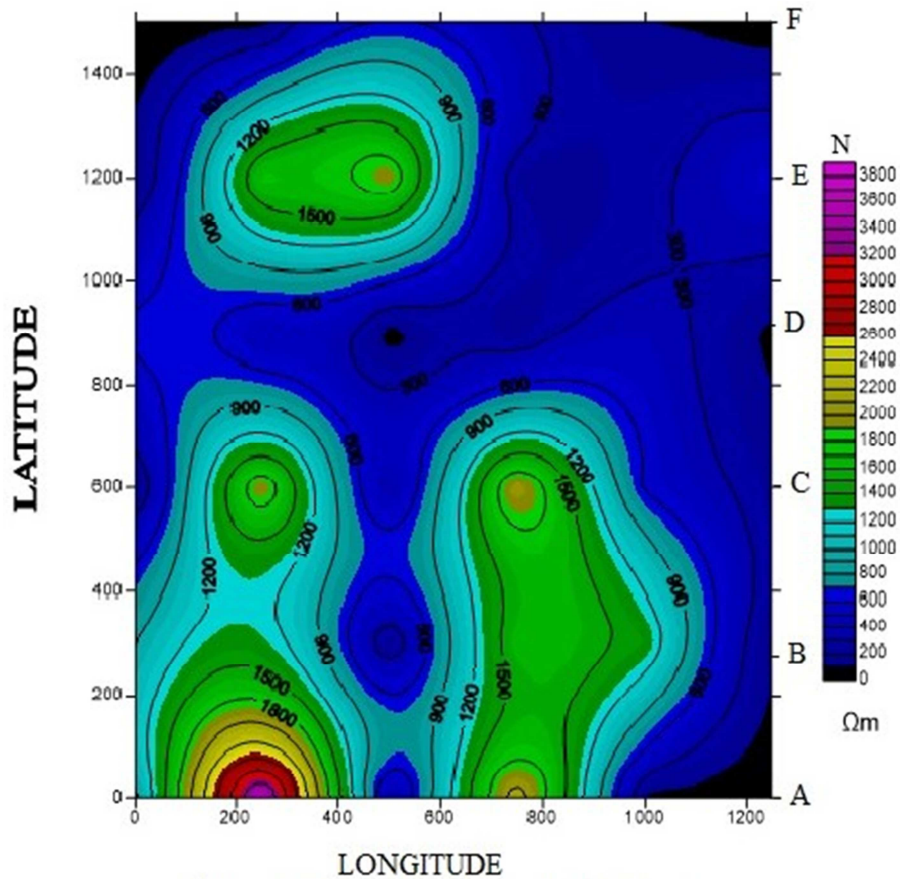


Figure A6. Iso-Resistivity maps for 30 m depth.

References

- [1] Abdullahi, N. K. and Iheakanwa, A. (2013). Groundwater detection in basement complex Northwestern Nigeria using 2D electrical resistivity and offset wenner techniques. *International Journal of Science and Technology*, 2 (5): 529-535.
- [2] Abiola, O., Enikanselu, P. A., & Oladapo, M. I. (2009). Groundwater potential and aquifer protective capacity of overburden units in Ado-Ekiti, Nigeria. *International Journal of Physical Sciences* 4 (3): 120–132.
- [3] Adetona, A. A., Salako, K. A., Abdulrashid, U. A., Rafiu, A. A., Ofor, N. P., Alhassan, D. U., & Jonah, S. A. (2013). Geophysical Investigation of Western Part of Federal University of Technology, Gidan Kwano Campus, Minna, Niger State, Using Electrical and Seismic Refraction Methods. *Natural and Applied Sciences Journal*: 11 (2).
- [4] Ajayi, C. O., & Hassan, M. (1990). The delineation of the aquifer overlying the basement complex in western part of the Kubanni Basin of Zaria (Nigeria). *Journal of Mining and Geology*, 26 (1), 117-124.
- [5] Ajayi, C. O & Anthony, C. W. (1988). Groundwater prospects in the basement complex rock of southwestern Nigeria. *Journal of African Earth Sciences*, 7 (1): 227–235.
- [6] Ajibade, A. C. (1980). The geology of the country around Zungeru, Northwestern state of Nigeria. Unpublished M. Sc. thesis, University of Ibadan, Ibadan, Nigeria.
- [7] Alagbe O A, Sunmonu L A, Adabanija M A (2013), Res. *Journal of Physical Sciences*, 1 (3), 1-5.
- [8] Alhassan, D. U., Mohammed, I. N., Bature, M., Kimpe, M. I., & Mohammed, A. (2015). Electrical resistivity survey for groundwater at Eye Zheba village. Off Bida- Minna road. *Journal of Applied Geology and Geophysics*, 3 (2): 49–53.
- [9] Alhassan, D. U., Obiora, D. N., & Okeke F. N. (2017). Geoelectrical investigation of groundwater potentials of northern Paiko, Niger state, northcentral Nigeria. *Journal of Earth Science*, 28 (1): 103–112.
- [10] Atakpo, E. A. and Ayolabi, E. A. (2009). Evaluation of Aquifer vulnerability and the protective capacity in some oil producing communities of western Niger Delta. *Journal of Environmentalist*, 29 (3): 318–322.
- [11] Balasubramanian, A. (2017). Methods of Groundwater exploration. Centre for advanced studies in earth science, University of Mysore. Mysore-6 publications.
- [12] Benson, A. K., Payne, K. L., & Stubben, M. A. (1997). Mapping groundwater contamination using dc resistivity and VLF geophysical methods; a case study. *Geophysics*, 62 (1), 80-86.
- [13] Chambers, J. E., Kuras, O., Meldrum, P. I., Ogilvy, R. D., & Hollands, J. (2006). Electrical resistivity tomography applied to geologic, hydrogeologic, and engineering investigations at a former waste-disposal site. *Geophysics*, 71 (6), B231-B239.

- [14] Dobrin, M. B., & Savit, C. H. (1960). Introduction to geophysical prospecting (Vol. 4). New York: McGraw-hill.
- [15] Ebong, E. D., Akpan, A. E., & Onwuegbuche, A. A. (2014). Estimation of geohydraulic parameters from fractured shales and sandstone aquifers of Abi (Nigeria) using electrical resistivity and hydrogeologic measurements. *Journal of African Earth Sciences*, 96, 99-109.
- [16] Grant, F. S., & West, G. F. (1965). Interpretation theory in applied geophysics. New York: McGraw-Hill.
- [17] Isaac, O. A., Ezikiel, A., Isaac, I. M., Jacob, B. J., Peace, E. A., Goodness, E. J., Nurudeen, R., & Peace N. J. (2022). Aquifer vulnerability and protective capacity test of Lokoja, Kogi state, Nigeria. *International Journal of Applied Chemical and Biological Sciences* 3 (4): 41-48.
- [18] Levi, I. N. (2011). 2D Resistivity Survey for Ground water Exploration in a Hard Rock Terrain: A Case Study of MAGDAS Observatory, Unilorin, Nigeria. *Asian Journal of Earth Sciences* 4 (1): 46-53 Lowerie, W. (1997). Fundamental of geophysics, electromagnetic surveying Cambridge University press. P. 220-223.
- [19] McCurry, P. (1976). The geology of the Precambrian to lower Paleozoic rocks of northern Nigeria, a review inc A, Kagbe (ed), geology of Nigeria, 15 - 39. Lagos, Elizabethan publishing co.
- [20] Mosuro, G. O., Omosanya, K. O., Bayewu, O. O., and Oloruntola, M. O. (2017). Assessment of groundwater vulnerability to leachate infiltration using electrical resistivity method. *Journal of applied Water Sciences* 7: 2195-2207. <https://doi.org/10.1007/s13201-016-0393-4>.
- [21] Ogungbemi, O. S., Badmus Ganiyu, O., Idowu, K. A., & Oluwatoyin, O. (2013). Geoelectric and electromagnetic methods for post foundation studies in a typical basement terrain. *Journal of Emerging Trends in Engineering and Applied Sciences*, 4 (6), 863-868.
- [22] Oladapo, M. I. and Akintorinwa, O. J. (2007). Hydrogeophysical study of Ogbese Southwestern, Nigeria. *Global Journal of Pure and Applied Sciences*. 131: 55-61.
- [23] Olorunfemi, M. O. & Fasuyi, S. A. (1993). Aquifer types and geoelectric/hydrogeologic characteristics of part of central basement terrain of Nigeria, (Niger state). *Journal of African Earth Sciences*. 16 (3): 157-160.
- [24] Olorunfemi, M. O., Ojo, J. S., & Akintunde, O. M. (1999). "Hydrogeophysical evaluation of the groundwater potential of Akure metropolis, southwestern Nigeria". *Journal of Mining and Geology*. 35 (2): 207-228.
- [25] Oluwafemi, O., & Oladunjoye, M. A. (2013). Integration of surface electrical and electromagnetic prospecting methods for mapping overburden structures in Akungba-Akoko, Southwestern Nigeria. *International Journal of Science and Technology*, 2 (1), 122-147.
- [26] Onyenweife, G. I., Nwozor, K. K., Nwike, I. S., Onuba, L. N., Egbunike, M. E. & Anakor, S. N (2020). Application of electrical resistivity method in estimating aquifer protective capacity of Akwa and its environs, Anambra state, Nigeria. *International Journal of Innovative Environmental Studies Research*, 8 (4): 1-17.
- [27] Oseji, J. O., Atakpo, E. A. & Okolie, E. C. (2005). Geoelectric investigation of the aquifer characteristics and groundwater potential in Kwale, Delta state, Nigeria. *Journal of Applied Sciences and Environmental Management*. 9: 157-160.
- [28] Parasnis, D. S. (1987). *Principle of Applied Geophysics*. London: Chapman and Hall Ltd.
- [29] Perez, J. W., & Barber, M. (1965). Distribution and chemical quality of groundwater in northern Nigeria. *Geological Survey of Nigeria Bulletin*, 36.
- [30] Salako, K. A., Adetona, A. A., Rafiu, A. A., Ofor, N. P., Alhassan, U. D., & Udensi, E. E. (2009). Vertical electrical sounding investigation for groundwater at the southwestern part (site A) of Nigeria Mobile Police barracks (MOPOL 12), David Mark road, Maitumbi, Minna. *Journal of Science, Education and Technology*, 2: 350-362.
- [31] Sharma S. P. & Baranwal, V. C. (2005) *Journal of Applied Geophysics*, 37, 155-166.
- [32] Sunmonu L A, Alagbe O A, (2011) *Internal Journal of Physics*, 3 (1), 70-75.
- [33] Sunmonu, L. A., Adagunodo, T. A., Olafisoye, E. R. & Oladejo, O. P. (2012). The groundwater potential evaluation at industrial estate Ogbomosho southwestern Nigeria. *RMZ-Materials and Geoenvironment*, 59 (4): 363-390.
- [34] Sunmonu, L. A., Adagunodo, T. A., Adeniji, A. A., Oladejo, O. P. & Alagbe O. A. (2015). Geoelectric delineation of aquifer pattern in crystalline bedrock. *Open Transactions on Geosciences*. 2 (1): 1-16.
- [35] Sunmonu, L. A., Adagunodo, T. A., Bayowa, O. G. & Erinle, A. V. (2016). Geophysical mapping of the proposed Osun state housing estate, Olupona for subsurface competence and groundwater potential. *Journal of Basic and Applied Research*. 2 (2): 27-47.
- [36] Telford, W. M., Geldart, L. P., Sheriff P. E., & Keys, D. A. (1976). *Applied Geophysics*. Cambridge: Cambridge University Press. Pp 1-5, 630-640.
- [37] Telford, N., Geldert, L. P., Sheriff, R. S., & Keys, D. A. (1990). *Applied Geophysics*, 2nd edition. Cambridge, University Press.
- [38] Tsepav, M. T., & Umar, M. A. (2016). Evaluation of aquifer protective capacity and soil corrosivity using geoelectrical method. *World Engineering and Applied Sciences Journal* 7 (3): 135-144.
- [39] Udensi, E. E., Ogunbanjo, M. I., Nwosu, J. E., Jonah S. A., Kolo, M. T., Onuduku, U. S., Crown, I. E., Daniyan, M. A., Adeniyi, J. O. & Okosun, F. A. (2005). Hydrogeological and Geophysical surveys for groundwater at designated premises of the main Campus of the Federal University of Technology, Minna. *Zuma Journals of Pure and Applied Science (ZJ PAS)*. 7 (1) pp. 52-58.
- [40] UNESCO, (2007). Record of illness and death from Water related diseases in the developing countries. *Journal of Medical Ethics* 33 (3): 150-154.
- [41] United Nations Educational, Scientific, and Cultural Organization. *World Water Balance and Water Resources of the Earth*. 1996.
- [42] Yadav, G. S., & Singh, S. K. (2007). Integrated resistivity surveys for delineation of fractures for ground water exploration in hard rock areas. *Journal of applied geophysics*, 62 (3), 301-312.

- [43] Henriet, J. P. (1976). Direct applications of the Dar Zarrouk parameters in ground water surveys. *Geophysical prospecting*, 24 (2), 344-353. Central part of Kaduna State, Nigeria. *Journal of Mining & Geology*, 35 (2), 189–206.
- [44] Dan-Hassan, M. A., & Olarinfemi, M. O (2015). Hydro-geophysical investigation of a basement terrain in the North-
[45] AB, A. I. (1999). ABEM Terrameter SAS 4000/SAS 1000 Instrument Manual. *ABEM Printed Matter*, (93101).

General Extreme Value Fitted Rainfall Non-Stationary Intensity-Duration-Frequency (NS-IDF) Modelling for Establishing Climate Change in Benin City

Masi G. Sam, Ify L. Nwaogazie*, Chiedozie Ikebude

Department of Civil and Environmental Engineering, University of Port Harcourt, Port Harcourt, Nigeria

Email address:

ifynwaogazie@yahoo.com (Ify L. Nwaogazie)

*Corresponding author

To cite this article:

Masi G. Sam, Ify L. Nwaogazie, Chiedozie Ikebude. General Extreme Value Fitted Rainfall Non-Stationary Intensity-Duration-Frequency (NS-IDF) Modelling for Establishing Climate Change in Benin City. *Hydrology*. Vol. 11, No. 4, 2023, pp. 85-93.

doi: 10.11648/j.hyd.20231104.13

Received: October 4, 2023; **Accepted:** November 7, 2023; **Published:** November 17, 2023

Abstract: The study focused on fitting non-stationary rainfall Intensity-Duration-Frequency (IDF) curves based on the General Extreme Value (GEV) distribution function to establish climate change existence in Benin City. The intensity levels were calculated, with the aid of the open-access R-studio software. Four linear behavioural parameter models considered for incorporating time as a covariate had the second model selected for producing the least corrected Akaike Information Criteria (AIC_C). The AIC_C varied from 370.30 to 125.20 for 15 and 1440 minutes, respectively, used in the calibration of the GEV equation. The computed non-stationary intensities produced higher values above those of stationary models, showing that the later IDF models undervalued extreme events. Differences of +15.24% (18.22 mm/hr), +9.4% (7.37 mm/hr), and +12.64% (12.78 mm/hr), for a 2, 10, and 50-year return periods, respectively, are serious underestimation from a stationary IDF model. Having extreme value differences could further aggravate the flood risk more than the design provision for the drainage facilities. The test statistic result confirmed a significant difference at a 95% confidence level between the non-stationary and stationary IDF curves, showing evidence of climatic change influenced by location as the time-variant parameter. The use of shorter-duration storms is advised for design purposes because they produce higher intensities and percentage differences in the extreme values, increasing the flood risk and infrastructural failures to induce climatic change in the study area.

Keywords: Rainfall, Time Series Data, Trend, Non-Stationary, Stationary, Curve Fitting

1. Introduction

Rainfall Intensity-duration-frequency (IDF) models are mathematical formulas derived in hydrology to calculate design storms in terms of the intensity of rainfall against its duration of fall for a given return period or, against the return period for a specified rainfall duration. The graphical representation of the mathematical formulation when values are assigned is known as IDF curves. IDF curves are very important for the design of different types of hydraulic facilities, for example, stormwater drainage systems, culverts, irrigation channels, and Dams.

Rainfall IDF models are applied in the conversion of the rainfall intensities into runoff volume in the design of hydraulic infrastructures. The stationary rainfall IDF model

assumes that extremes do not vary significantly over time.

Non-stationary IDF modelling applies dynamic time series data to allow for the use of the sample mean, variance and covariance changes over time. The non-application of Non-stationary concepts in hydrological modelling leads to inaccurate results [1]. The measured rainfall data is checked for a trend to ascertain the presence of dynamic sequential behaviour. When the trend is significant, the location parameters can be evaluated using the non-stationary assumption. The state-of-the-art studies are on the development of IDF curves based on the non-stationary concept [1-4]. Bougadis and Adamowski [2] opined that the simple scaling process of rainfall IDF relationship is more efficient with more accurate estimates in non-stationary IDF modelling than from the stationary approach.

A framework for evaluating climate change impacts on natural and developed infrastructures applying bias-corrected multi-model simulations on historical and projected precipitation extremes was outlined [5]. Changes in rainfall IDF curves and their uncertainty bounds were derived using a non-stationary model integrating Bayesian Inference. Further studies by several authors on IDF modelling show that the Non-stationary framework for IDF modelling gives a better fit to the sample data than the stationary method [1, 6].

This study is focused on the development of a 24-hourly annual maximum series (AMS) non-stationary rainfall IDF model for Benin City using a statistical approach to fit the general extreme value (GEV) distribution function with the aid of non-stationary behavioural parameters to establish climate change existence in the study area. The basic steps

for developing a 24-hourly GEV distribution function-based non-stationary model and its stationary-based parameter model counterpart are summarized and presented in a flowchart [7].

2. Materials and Methods

2.1. Study Area

Benin City is the capital of Edo State in the South-Central region of Nigeria. It is located between longitudes $5^{\circ}34'$ E – $5^{\circ}44'$ E and latitudes $6^{\circ}52'$ N – $6^{\circ}21'$ N, as shown in Figure 1. See details of the study area description as presented in our earlier publication [8].

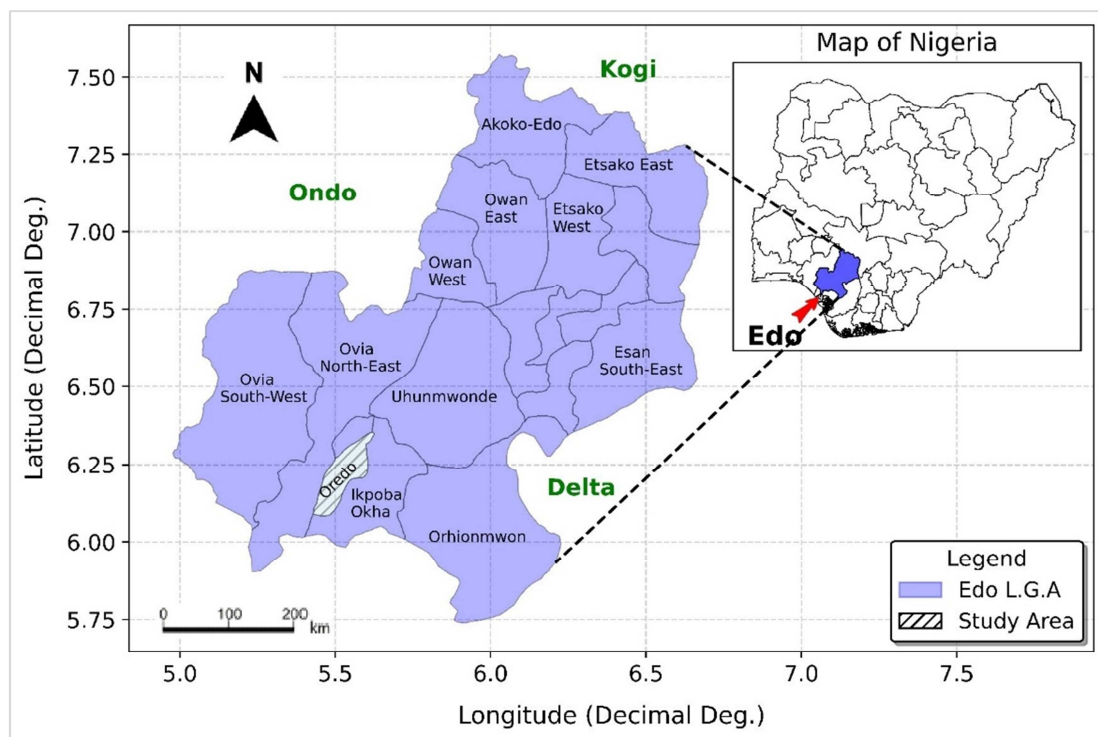


Figure 1. Map of Edo State showing the study area - Benin City.

2.2. Data Collection

The observed rainfall data for this study were recorded for about three and a half decades precisely 36 years (1982-2017), from the Nigeria Meteorological Agency (NIMET) gauge station at Benin City. The data collected were sorted out by extracting the 24-hourly annual maximum series (AMS) rainfall time series data from the maximum monthly series (MMS) for each year for the rest of the 36-year interval. The 36-year 24-hourly AMS data were further downscaled into shorter durations using the relationships established by the Indian Meteorological Department (IMD) and the Modified Chowdhury Indian Meteorological Department (MCIMD) scaling methods. See more details of the calibration and scaling process in the author's earlier publications [8, 9].

2.3. Climatic Trends Check in the Time Series Data

Non-stationary IDF modelling (NS-IDF) requires the testing for non-stationarity signals on the measured rainfall data as a precondition. For the detection of whether the trends are statistically significant or not in the time series data, the rank-based non-parametric Mann-Kendall (MK) method with the Sen's Slope Estimator (SSE) was applied to the data [10-12]. The details of the procedure can be found in our earlier publications [8, 13].

2.4. Fitting Non-Stationary IDF Curves with Generalized Extreme Value (GEV) Distribution Function

The introduction of the time-dependent parameters into the general intensity-duration-frequency relationship was the

basis of the GEV distribution functions [14]. The standard cumulative distribution function (CDF) of the GEV is shown in Equation (1) [15], with more information on the procedure also available in our earlier study [8].

$$F(x) = \exp \left[- \left(1 + \xi(t) \frac{x - \mu(t)}{\sigma(t)} \right)^{-1/\xi(t)} \right] \text{ for } \xi \neq 0 \quad (1)$$

Where $F(x)$ = Cumulative Distribution Function, ξ = shape parameter, μ = mean and σ = standard deviation.

2.5. Deriving GEV Time-Variant Parameter Models

The extreme value theory of stationary random series assumes that statistical properties of extremes such as distribution parameters $\theta = (\mu, \sigma, \xi)$ are independent of time [16]. In contrast, for a non-stationary process, the parameters of the fundamental distribution function are time-dependent and have time-varying properties [17]. To represent a dynamic distribution, the location and scale parameters are assumed to be linear functions of time to account for non-stationarity, with the shape parameter kept constant [4, 14, 16, 18, 19]. Thus, the time-varying covariates are incorporated into GEV location and both location and scale parameters respectively, thereby describing trends as a linear function of time in years.

This study considered four different linear model combinations of the GEV parameters by assuming a case of linear trend for location and linear trend for scale parameters and their different combinations as in the literature [9, 20]. We have Model type $GEV_t - 0$ = where all parameters are assumed constant for stationary case; $GEV_t - I$ is $\mu(t) = \mu_o + \mu_1 t$; $GEV_t - II$ is $\sigma(t) = \sigma_o + \sigma_1 t$; and $GEV_t - III$ is $\mu(t) = \mu_o + \mu_1 t$, and $\sigma(t) = \sigma_o + \sigma_1 t$. Given a typical rainfall duration of values $X = X_1, X_2, \dots, X_n$, for n years of the annual maximum time series. The log-likelihood for the Stationary is expressed as written in Equation (2) based on the condition of Equation (3).

$$\log L(\mu, \sigma, \xi | X) = -n \log \sigma - \left(1 + \frac{1}{\xi} \right) \sum_{i=1}^n \log \left[1 + \xi \left(\frac{x_i - \mu}{\sigma} \right) \right] - \sum_{i=1}^n \left[1 + \xi \left(\frac{x_i - \mu}{\sigma} \right) \right]^{-1/\xi} \quad (2)$$

$$\text{For } \xi \neq 0 \text{ and } 1 + \xi \left(\frac{x_i - \mu}{\sigma} \right) > 0, \quad (3)$$

Where, the Maximum Likelihood Estimates (MLEs) parameter values allow for the extension to the non-stationary case, in which the parameters of the GEV distribution depend on time, t [21]. To obtain the parameters of extreme distributions as the GEV is by minimizing the negative log-likelihood function evaluated using iterative numerical method.

Sequel to the derivation of the GEV parameter model values, the next step is to identify which of the GEV parameter models best represents the original data. To select the best model, the corrected Akaike Information Criteria (AICc) is preferable, because it penalizes the minimized negative log-likelihood for the number of parameters

estimated [21]. The AICc is recommended in practical applications because it outperforms the original AIC and helps to avoid over-fitting the data [22].

2.6. Deriving Stationary & Non-Stationary Intensity Duration Frequency Curves

The fitting of Non-stationary IDF curves based on the GEV distribution function requires the determination of the best GEV behavioural extreme parameters for substitution into the CDF formula in Equation (1). So that to enable the evaluation of the rainfall intensities, x_T , assuming stationarity (i.e., constant value) of the behavioural parameters, Equation (1) is solved by inversion of the CDF to have the subject of the equation as written in Equation (4) [3, 15]:

$$x_T = \left[\left(-\frac{1}{\ln P} \right)^\xi - 1 \right] x \frac{\sigma}{\xi} + \bar{\mu}, (\xi \neq 0) \quad (4)$$

Where x_T = rainfall intensity exceedance value, and T = return period. The return periods and return levels of extremes in Equations (4) are determined by expressing return levels as a function of the return period T as in Equation (5) [6]

$$T = \frac{1}{1-P} \quad (5)$$

Where p is the non-exceedance probability of occurrence in a given year, assumed constant under the stationary IDF concept. Also, for each return period and duration, the intensity values are calculated with IDF curves plotted.

However, by estimating the model parameters on the conditions of Non-stationarity in terms of the behavioural parameter extremes, it can be extended to estimate the Non-stationary return level or rainfall intensity as given in Equation (6):

$$\bar{x} = Q_K(\mu_{t1}, \mu_{t2}, \dots, \mu_{tn}), (\mu(t) = \mu_1 t + \mu_o)$$

$$x_T = \left[\left(-\frac{1}{\ln P} \right)^\xi - 1 \right] x \frac{\sigma}{\xi} + \bar{\mu}, (\xi \neq 0) \quad (6)$$

Where x_T = rainfall intensity exceedance value, and T = return period. The return levels are also translated into intensities for each return period and duration, with the IDF curves plotted.

For example, let us compute the rainfall intensity values for both Stationary and Non-stationary GEV fitted Curve given 15-minute rainfall at 2-year return periods for a daily annual time series data collected for 30 years just like the case of Benin City.

For Stationary Case – Using the intensity formula from Equation (4) with the computed GEV parameters from Table 1: location, $\mu=146.178$; scale, $\sigma = 35.22$, and shape, $\xi = 0.0304$ for $T = 2$ years return period. The rainfall intensity, x_T can be obtained by making necessary substitutions;

$$T = \frac{1}{1-P} \Rightarrow P = 1 - \frac{1}{T} = \frac{2-1}{2} = \frac{1}{2} = 0.5 \quad ; \quad \text{ie, From Equation (5), so that the rainfall intensity.}$$

$$x_T = \left[\left(-\frac{1}{\ln 0.5} \right)^{0.0304} - 1 \right] \times \frac{35.22}{0.0304} + 146.178 = 12.98 + 146.178 = 159.16 \text{ mm/hr}$$

For Non-stationary Case - From Table 1, the GEV_t - I parameter model is the best selected with the least AIC_c and the parameters are obtained as follows; Location, $\mu(t) = 118.019 + 1.495t$; Scale, $\sigma(t) = 28.11$, and Shape, $\xi = 0.1722$, with data collection time, $t = 36$ years. Substituting the time, $t = 30$ years we have; $\mu(t) = 118.019 + 1.495 \times 36 = 171.849$, $\sigma(t) = 28.11$, and $\xi = 0.1722$.

Therefore, substituting the values of the calculated parameter estimates into Equation (6) for Non-stationary rainfall intensity computation for 2 year return period for the 15-minute duration we have;

$$x_T = \left[\left(-\frac{1}{\ln 0.5} \right)^{0.1772} - 1 \right] \times \frac{28.11}{0.1722} + 171.849 = 10.634 + 171.849 = 182.48 \text{ mm/hr}$$

2.7. Comparing Non-Stationary Against Stationary Predicted Rainfall Intensities

Graphical plots of computed rainfall intensities against durations were carried out for a given return period, with the return period against duration at a given duration. The statistically significant differences between the best non-stationary model and the stationary models were evaluated using the Wilcoxon signed rank sum non-parametric test. Acceptance is given to the null hypothesis if the critical value corresponding to alpha, $\alpha = 0.05$ at reduced sample size, n , were greater than the computed statistic value. The statistical significance of the best non-stationary model compared to the stationary model was measured by the p-value of the Wilcoxon signed rank statistic test at a 5% level of significance [24].

3. Results

3.1. Generalized Extreme Value (GEV) Behavioural Parameter Models Evaluation

Thirty-six years of measured rainfall data were collected and sorted into 24-hourly Annual Maximum Series (AMS) for each year. The data were disaggregated using the IMD and MCIMD downscaling models into shorter durations as in our earlier published work [9, 13].

The condition for non-stationary IDF modelling requires evidence of trend existence in the time series data which was a positive trend. The performances of the different linear parameter models selected are shown in Table 1. They are expressed as functions of time with their derived values. The best in performance of the non-stationary models was chosen based on the corrected Akaike Information Criteria (AIC_c)

obtained to represent the time series data. The selected linear parameter models were substituted into Equations (4) and (6) for the evaluation of the rainfall intensities.

3.2. Fitting GEV Distribution Function IDF Curves

The open-access R Studio software package was used to develop the rainfall IDF curves [25]. The CDF of the GEV formula given in Equation (1) was used for fitting both the stationary and the non-stationary IDF curves. The GEV distribution has the combination of the Gumbel, Frechet and Weibull distributions which constitutes the necessary and required condition expressed in Equation (3). Thus, the formulation of Equation (1) enabled the optimization of the log-likelihood function of Equation (2) which allowed for its extension to the non-stationary modelling, in which the parameters of the GEV distribution depend on time t . The GEV Equation (1) when inverted results in Equations (4) & (6) used for the computation of the rainfall intensity values. The parameters of the GEV formula were obtained by minimizing the negative likelihood function through an iterative numerical approach. Subsequently, Non-stationarity was introduced by expressing one or more of the parameters of the GEV as a function of time that were selected.

The rainfall intensity values were computed for the non-stationary IDF curves based on the selected best model. The linear model with the least AIC_c presented in Table 1 is GEV_t-I., on the basis for which the rainfall intensities were estimated. The results of the rainfall intensities computed for both the stationary and non-stationary models were plotted together. Figure 2 shows the plots of the GEV distribution fitted non-stationary and stationary against duration IDF curves on the same graph paper for given return periods, while Figure 3 shows the GEV distribution fitted non-stationary and stationary against return period IDF curves plotted on the same graph paper for given durations, respectively.

3.3. Percentage Differences Between Non-Stationary and Stationary IDF Curves

The graphical plots of rainfall intensity values against duration, and return period presented in Figures 2 and 3, respectively, show a visual difference between the non-stationary and the stationary models at each plotting point. However, it is important to verify if the differences were statistically significant. The computed rainfall intensity values for stationary and non-stationary obtained were evaluated to obtain their percentage differences. The Wilcoxon non-parametric paired test of significance was carried out to verify this fact if the percentage differences were significant at a 95% Confidence level.

Table 1. Performance of GEV Parameters Evaluated for Non-Stationary and Stationary Models for Benin.

Time (mins)	Model	Location Parameter	Scale	Shape Parameter	AIC	AIC _c
15	GEV _t -0	146.178	35.22	0.0304	376.74	377.49
	GEV _t -I	118.019 + 1.495t	28.11	0.1722	369.01	370.30
	GEV _t -II	149.704	45.231 - 0.653t	0.1842	377.13	378.42
	GEV _t -III	117.743 + 1.511t	27.785 + 0.0194t	0.1718	371.011	373.01

Time (mins)	Model	Location Parameter	Scale	Shape Parameter	AIC	AIC _c
30	GEV _t -0	84.753	20.997	0.0297	339.47	340.22
	GEV _t -I	68.003 + 0.890t	16.773	0.1717	331.71	333.00
	GEV _t -II	89.937	27.110 - 0.395t	0.1856	339.86	341.15
	GEV _t -III	67.854 + 0.899t	16.597 + 0.0094t	0.1713	333.71	335.71
45	GEV _t -0	61.751	15.493	0.0301	317.57	318.32
	GEV _t -I	49.407 + 0.655t	12.773	0.1725	309.86	311.15
	GEV _t -II	63.326	19.978 - 0.290t	0.1861	317.967	319.26
	GEV _t -III	49.280 + 0.662t	12.237 + 0.0073t	0.1722	311.857	313.86
60	GEV _t -0	49.345	12.487	0.0305	302.036	302.79
	GEV _t -I	39.405 + 0.527t	9.971	0.172	294.33	295.62
	GEV _t -II	50.6118	16.074 - 0.233t	0.185	302.429	303.72
	GEV _t -III	39.293 + 0.534t	9.849 + 0.0066t	0.1719	296.327	298.33
120	GEV _t -0	28.809	7.447	0.0295	264.801	265.55
	GEV _t -I	22.868 + 0.316t	5.947	0.1707	257.055	258.35
	GEV _t -II	29.57	9.594 - 0.129t	0.1844	265.199	266.49
	GEV _t -III	22.802 + 0.319t	5.876 + 0.0039t	0.1704	259.052	261.05
360	GEV _t -0	12.339	3.277	0.0284	205.655	205.66
	GEV _t -I	9.737 + 0.138t	2.623	0.1678	197.984	197.98
	GEV _t -II	12.671	4.217 - 0.061t	0.183	206.05	206.05
	GEV _t -III	9.706 + 0.140t	2.589 + 0.0018t	0.1675	199.98	201.98
720	GEV _t -0	7.258	1.952	0.0289	168.386	169.14
	GEV _t -I	5.681 + 0.084t	1.551	0.1758	160.488	161.78
	GEV _t -II	7.464	2.529 - 0.037t	0.1878	168.745	170.04
	GEV _t -III	5.677 + 0.00838t	1.545 + 0.0003t	0.1754	162.488	164.49
1440	GEV _t -0	4.268	1.173	0.0269	131.606	132.36
	GEV _t -I	3.331 + 0.0497t	0.9358	0.168	123.911	125.20
	GEV _t -II	4.387	1.5078 - 0.022t	0.1796	132.016	133.31
	GEV _t -III	3324 + 0.0501t	0.9304 + 0.0004t	0.1664	125.99	127.99

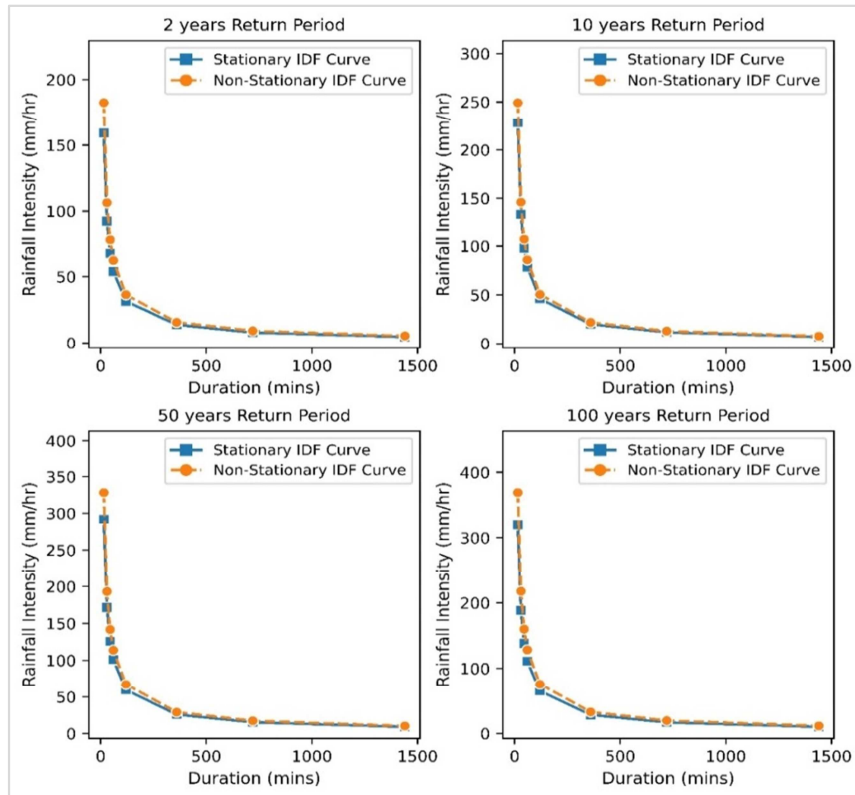


Figure 2. GEV Distribution Fitted Non-stationary versus Stationary IDF Curves for Different Return Periods for Benin.

Table 2. Percentage Difference of Rainfall Intensities between Non-Stationary and Stationary IDF Curves for Benin.

Duration (mins)	Return Period (years)					
	2	5	10	25	50	100
15	14.65±	9.85	9.15	10.31	12.37	15.30
30	15.04	10.08	9.36	10.53	12.60	15.57

Duration (mins)	Return Period (years)					
	2	5	10	25	50	100
45	15.13	10.11	9.39	10.63	12.67	15.67
60	15.24	10.14	9.40	10.55	12.64	15.62
120	15.53	10.36	9.54	10.67	12.75	16.06
360	13.43	10.54	9.72	10.77	12.80	15.72
720	16.29	10.73	9.91	11.23	13.44	16.60
1440	16.38	10.89	9.87	10.87	13.09	16.08
Av. %tage Difference	15.21	10.34	9.54	10.69	12.79	15.83

± Percentage Difference of Rainfall Intensities

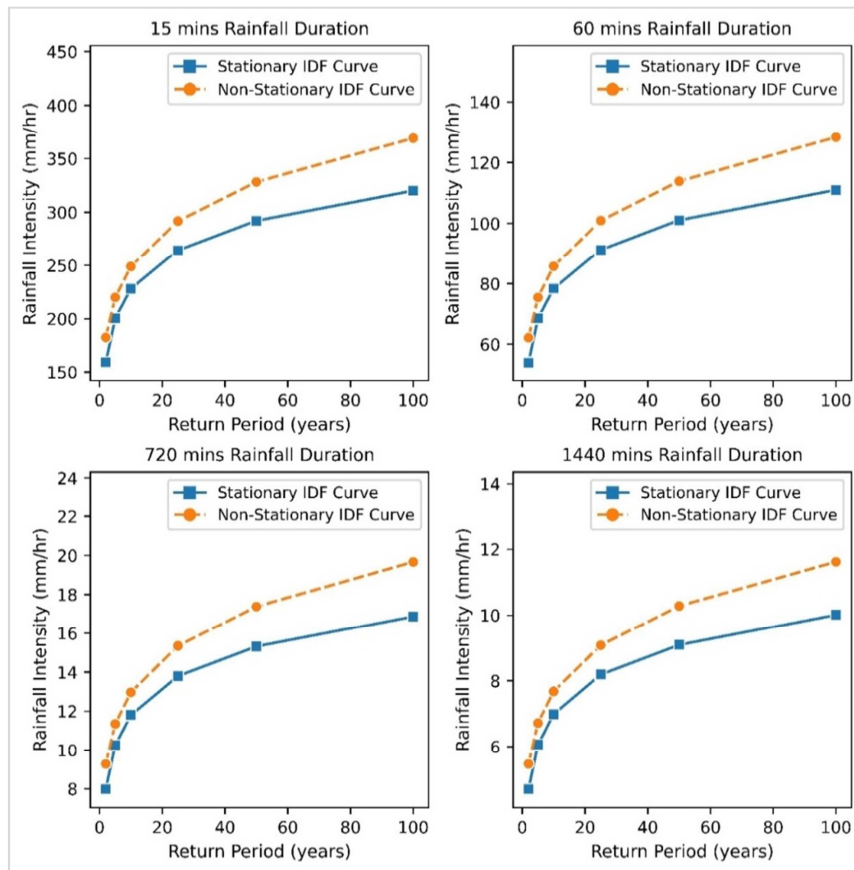


Figure 3. GEV Distribution Fitted Non-Stationary versus Stationary IDF Curves for Different Durations for Benin.

The two-tailed statistic test was carried out for rainfall intensities against duration for a given return period and rainfall intensities against return period for the given duration. The Wilcoxon statistic test result was compared with the critical p-value at alpha, ∞ - value of 5% level of significance.

4. Discussion

4.1. Analysis of Evaluated GEV Behavioural Parameter Models

This research study was carried out based on 24-hourly measured annual maximum series (AMS) data constructed using the Modified Chowdhury Indian Meteorological Department (MCIMD) downscaling method. The MCIMD downscaling models produced higher rainfall intensity values than other models for different shorter durations of 0.25 to

1.0 hours typical of urban drainage, and 2 to 24 hours longer duration applied in large-scale or rural infrastructural designs. The downscaled rainfall intensities (mm/hr) plotted against duration (years) showed a strong positive (i.e., increasing) trend as obtained in our earlier publication [13].

The behavioural parameters considered were scale, location, and shape, expressed in four different linear models for the integration of time as co-variate in the calibration of the GEV distribution Equation (1). The GEVt – 0 is the first linear model applied at constant values of the various parameters, the same as the stationary assumption model of the Gumbel Extreme Value 1 (GEVt-1). The second model, GEVt – I have time as a co-variate with location as the behavioural parameters while the scale and shape parameters remain constant. The GEVt – II is the third model, having time as a co-variate with scale parameters, while location and shape parameters are constant. The fourth model, GEVt – III has the shape parameter constant while the time is co-varying

with both location and scale parameters.

For the Benin City meteorological station, the best-performed linear model was the model with the least AIC_C , chosen as reasonable and representing the non-stationarity better. Therefore, the second model, $GEV_t - I$ was chosen as the best parameter model for the calculation of the parameters required for calibration of the GEV Equation (1). The equation was adopted in the calculation of the non-stationary rainfall intensities for various durations in a given return period, and also for different return periods in a given duration.

4.2. The Analysis of Evaluated GEV Distribution Function Fitted IDF Curves

The R-studio software was applied for all the computations to obtain the rainfall IDF curves fitted based on the GEV distribution function. The formula for obtaining the cumulative distribution function for the GEV distribution has a family of three distribution functions controlled by the shape function when it is either zero, more than zero or less than zero, given in Equation (1). The expression of the equation into the log-likelihood form in Equation (2) provided the basis for computing the parameters of the GEV distribution function for both stationary, vis-a-vis the extension of the principles to the non-stationary condition where time is integrated as a covariate [22]. The parameters were, therefore, calculated on the satisfactory condition of Equation (3) through optimization of the minimization of the negative log-likelihood achieved by iteration.

The intensity levels for various downscaled durations for any given return period were computed from Equation (1), inverted to derive Equation (6) which were applied with the values of the best linear parameter model substituted to obtain the non-stationary intensities. The intensities of the stationary model were also calculated based on model 1, that is, $GEV_t - 0$ which is the stationary counterpart. The intensity levels computed for both stationary and Non-stationary models were plotted against duration for a given return period on the same normal graph paper, to obtain the IDF curves shown in Figure 2. Also, the plot of the computed intensities was made against the different return periods for a given duration presented in Figure 3.

4.3. Analysis of Percentage Difference Between Non-Stationary & Stationary IDF Curves

The plotted curves in Figures 2 and 3 show glaring visual differences for intensity levels against both return levels and duration, respectively. However, the plots in Figure 2 may require further confirmation in terms of the percentage differences. The calculated percentage differences presented in Table 2 showed that for the plots in Figure 2, the intensity values for the non-stationary distributions produced higher values above those of stationary distributions for Benin City. This implies that the stationary distribution function delivers IDF curves that underestimate extreme events as in the literature [3]. For example,

considering a 1-hr storm duration event gave the percentage difference between the non-stationary and stationary extreme rainfall of +15.24% (18.22 mm/hr), +9.4% (7.37 mm/hr), and +12.64% (12.78 mm/hr), for a 2, 10, and 50 year return periods, respectively. Such differences of 18.22 mm/hr, 7.37 mm/hr, and 12.78 mm/hr, rainfall intensities in a 1-hour duration storm for a small catchment area could lead to serious underestimation of the peak flood from a stationary IDF curve. The obtained extreme value differences could worsen the flood risk more than the design provision. These under estimations signify that if the stationary intensities were applied for infrastructural designs, such a project may not contain extreme hydrologic events as indicated by the non-stationary counterpart to guarantee safety for some particular return periods [3, 4, 20].

Further observation revealed that the intensity of rainfall indicated higher differences between non-stationary and stationary at short durations. Because, at a 2-year return period, the rainfall intensity differences between the distributions varied from 8.22 mm/hr to 1.3 mm/hr for 1-hour and 12-hour storm durations, respectively. While at the 100-year return period, the intensity difference at 1 hour is 17.34 mm/hr and reduces to 2.8 mm/hr at 12-hour storm duration, and tends to zero (1.62 mm/hr) at 24-hour storm. This result suggests that emphasis should be laid on shorter duration storm for design purposes because it occurs with higher intensities showing higher differences in the extreme values, which have the potential of increasing the flood risk that causes hydrological facilities failure, consistent with an earlier study [8].

The study also observed differences between the non-stationary and stationary intensities in Benin City to have increased with higher durations from 15 min to 1440 min for 2 and 5-year shorter return periods, but reduced in value at 1440 min for 10, 25, 50, and 100 years return period. This proves that longer-duration events have not changed much for concern over the succeeding years, while shorter-duration events persistently increased [3].

To further establish the existence of a statistically significant difference between both intensity distributions, performance evaluation for a two-tailed sample using Wilcoxon signed rank sum statistic was carried out for given return periods, and also for given duration. The Wilcoxon signed rank sum test statistic calculated was 0.0143 for all return periods, which is less than the critical p-value at alpha, ∞ value = 0.05. Also, the Wilcoxon signed rank sum test statistic was calculated as 0.0360 for all durations. These values computed being less than the critical p-value at a 5% level of significance, the result affirms that there are significant statistical differences between the non-stationary and stationary IDF curves.

5. Conclusion

This study has proven that Benin City with a positive trend in the time series data requires non-stationary IDF modelling. Among four linear behavioural parameter

models considered for incorporating time as a covariate. The second model, GEVt – I with time as a covariate and location as the behavioural parameter dominating, while the scale and shape parameters are constant in the study area. The linear model produced the least corrected Akaike Information Criteria (AICC) varying between 370.30 to 125.20 for 15 and 1440 minutes, respectively, and was selected for calibration of the GEV equation for the computation of intensity levels. The computed intensities showed that the non-stationary curves were higher than the stationary curves, indicating that the computed stationary intensities underestimate extreme storm events. Where, a 1-hr storm duration rainfall event produced a percentage difference between the non-stationary and stationary of +15.24% (18.22 mm/hr), +9.4% (7.37 mm/hr), and +12.64% (12.78 mm/hr), for a 2, 10, and 50 year return periods, respectively; and for a small watershed could lead to serious underestimation of the peak flood. The test statistic result proved a significant difference at a 95% confidence level between the non-stationary and stationary IDF curves.

This study also shows emphasis should be on shorter duration storms for design purposes because they produced higher intensities and higher percentage differences in the extreme values which could increase the flood risk and infrastructural failures.

Conflicts of Interest

The authors declare no conflicts of interest.

References

- [1] Ouarda, T. B. M. J., Yousef, L. A. and Charron, C. (2019) Non-stationary Intensity-Duration-Frequency Curves Integrating Information Concerning Tele-connections and Climatology <https://doi.org/10.1002/joc.5953>
- [2] Adamowski, K. and Bougadis, J. (2006) Detection of Trends in Annual Extreme Rainfall. *Hydrological Processes*, 17: 3547-3560. <https://doi.org/10.1002/hyp.1353>
- [3] Cheng, L. and AghaKouchak, A. (2014) Non-Stationarity Precipitation Intensity- Duration-Frequency Curves for Infrastructure Design in a Changing Climate. *Science Reports*, 4, Article No. 7093, 1-6. <https://doi.org/10.1038/srep07093>
- [4] Ganguli, P. and Coulibaly, P. (2017) Does Non-Stationary in Rainfall Require Non-Stationary Intensity-Duration Frequency Curves? *Hydrology and Earth System Sciences*, 21, 6461-6483. <https://doi.org/10.5194/hess-21-6461-2017>.
- [5] Aghakouchak, A., Ragno, E., Love, C. and Mofkharhi, H. (2018) Projected Changes in California's Precipitation Intensity-Duration-Frequency Curves. California's Fourth Climate Change Assessment, California Energy Commission. Pub. No.: CCCA4-CEC-2018-005.
- [6] Ren, H., Hou, Z. J., Wigmosta, M., Liu, Y. and Leung, L. R. (2019) Impacts of Spatial Heterogeneity and Temporal Non-Stationarity of Intensity-Duration-Frequency Estimates – A Case Study in a Mountainous California-Nevada Watershed. *Water*, 11, 1296. <https://doi.org/10.3390/w11061296>
- [7] Sam, M. G., Nwaogazie, I. L. and Ikebude, C. 2023a. Establishing Climatic Change on Rainfall Trend, Variation and Change Point Pattern in Benin City, Nigeria. *International Journal of Environment and Climate Change*, 13 (5): 202-212. <https://doi.org/10.9734/IJECC/2023/v13i51761>.
- [8] Sam, M. G., Nwaogazie, I. L., Ikebude, C., Iyang, U. J. and Irokwe, J. O. 2023b Modeling Rainfall Intensity-Duration-Frequency (IDF) and Establishing Climate Change Existence in Uyo-Nigeria Using Non-Stationary Approach. *Journal of Water Resource and Protection*, 15, 194-214. <https://doi.org/10.4236/jwarp.2023.155012>
- [9] Sam, M. G., Nwaogazie, I. L. and Ikebude, C. (2021). Improving Indian Meteorological Department Method for 24-hourly Rainfall Downscaling to Shorter Durations for IDF Modeling. *International Journal of Hydrology*, 5 (2), 72-82. <https://doi.org/10.15406/ijh.2021.05.00268>
- [10] Yue, S. and Wang, C. (2004) The Mann-Kendall Test-Modified by Effective Sample Size to Detect Trend in Serially Correlated Hydrological Series. *Water Resources Management*, 18 (3), 201-218. <https://doi.org/10.1023/B:WARM.0000043140.61082.60>
- [11] Ahmad, I., Tango, D., Wang, T., Wang, M. and Wagan, B. (2015) Precipitation Trends over Time Using Mann- Kendall and Spearman's Rho Tests in Swat River Basin, Pakistan, *Advances in Meteorology*, 2015, Article ID: 431860. <https://doi.org/10.1155/2015/431860>.
- [12] Okafor, G. C., Jimoh, O. D. and Larbi, K. I. (2017) Detecting Changes in Hydro-Climatic Variables during the Last Four Decades (1975-2014) on Downstream Kaduna River Catchment, Nigeria. *Atmospheric and Climate Sciences*, 7, 161-175. <https://doi.org/10.4236/acs.2017.72012>
- [13] Sam, M. G., Nwaogazie, I. L. and Ikebude, C. (2022). Climate Change and Trend Analysis of 24-Hourly Annual Maximum Series Using Mann-Kendall and Sen's Slope Methods for Rainfall IDF Modeling. *International Journal of Environment and Climate Change*, 12 (2), 44-60. <https://doi.org/10.9734/ijecc/2022/v12i230628>
- [14] Cheng, L., AghaKouchak, A. Gilleland, E. and Katz, R. W. (2014) Non-Stationary Extreme Value Analysis in a Changing Climate. *Climate Change*, 127, 353-369. <https://doi.org/10.1007/s10584-014-1254-5>
- [15] Coles, S., Bawa, J., Trenner, L. and Dorazio, P. (2001). *An Introduction to Statistical Modeling of Extreme Values*. Springer, London. <https://doi.org/10.1007/978-1-4471-3675-0>
- [16] Renard, B., Sun, X. and Lang, M. (2013) Bayesian Methods for Non-Stationary Extreme Value Analysis. In *Extremes in a Changing Climate*; Springer: Dordrecht. The Netherlands, pp. 39-95. https://doi.org/10.1007/978-94-007-4479-0_3
- [17] Meehl, G. A. et al. (2000) An introduction on trends in Extreme Weather and Climate Events: Observations, Socioeconomic Impacts Terrestrial Ecological Impacts and Model Projections. *B Am Meteorol Soc*. 81, 413-416. [https://doi.org/10.1175/1520-0477\(2000\)081<0413:AITTIE>2.3.CO;2](https://doi.org/10.1175/1520-0477(2000)081<0413:AITTIE>2.3.CO;2)
- [18] Katz, R. (2010) Statistics of Extremes in Climate Change. *Climate Change*, 100, 71-76. <https://doi.org/10.1007/s10584-010-9834-5>
- [19] Gilleland, E. and Katz, R. W. (2011) New Software to Analyze How Extremes Change Over Time. *EOS Trans. Am. Geophys. Union*. 92, 13-14. <https://doi.org/10.1029/2011EO020001>

- [20] Silva, D. F., and Simonovic, S. P. (2020) Development of Non-Stationary Rainfall Intensity Duration Frequency Curves for Future Climate Conditions. Water Resources Research Report No: 106. Department of Civil and Environmental Engineering, Western University, Canada, 43 pages. ISBN (print) 978-0-7714-3137-1; (Online) 978-0-7714-3138-8.
- [21] Katz, R. W. et al. (2013) Statistical methods for nonstationary extremes. In: Kouchak, A. A., et al. (Eds.). *Extremes in a Changing Climate: Detection, Analysis and Uncertainty*. Springer, Dordrecht, pp. 15-37. https://doi.org/10.1007/978-94-007-4479-0_2
- [22] Sugahara, S., and Rocha, R. P. and Silveira, R. (2009) Non-stationary frequency analysis of extreme daily rainfall in Sao Paulo, Brazil, 29, 1339–1349. <https://doi.org/10.1002/joc.1760>.
- [23] Cooley, D. (2013) Return Periods and Return Levels under Climate Change. *Extremes in a Changing Climate*, Springer, Netherlands. https://doi.org/10.1007/978-94-007-4479-0_4
- [24] Kothari, C. R. and Garg, G. (2014) *Research Methodology: Methods and Techniques*. 3rd ed. New Age International (P) Limited, Publishers, New Delhi.
- [25] RStudio Team (2020) RStudio: Integrated Development for R. RStudio, PBC, Boston, MA URL <http://www.rstudio.com/>.

Hydrology (HYD)

<http://www.sciencepublishinggroup.com/j/hyd>

Hydrology (HYD), a peer-reviewed open access journal published bimonthly in English-language, provides an international forum for publishing the study of the movement, distribution, and quality of water on Earth and other planets, including the hydrologic cycle, water resources and environmental watershed sustainability. It aims to publish definitive and original research papers of high standard, containing material of broad interest and of significant contribution to Hydrology, with emphasis being placed on hydrometeorology, surface hydrology, hydrogeology, drainage basin management and water quality, where water plays the central role.

Subject Coverage

The topics related to this journal include but are not limited to:

- Drainage basin management
- Groundwater
- Hydrogeology
- Hydrometeorology
- Infiltration
- Integrating measurement and modelling
- Modelling
- Precipitation and evaporation
- Prediction
- Remote sensing
- Soil moisture
- Statistical hydrology
- Surface hydrology
- Surface water flow

Notes for Intending Authors

Publishing your research in a Science Publishing Group journal is simple and efficient. Please use online submission system:

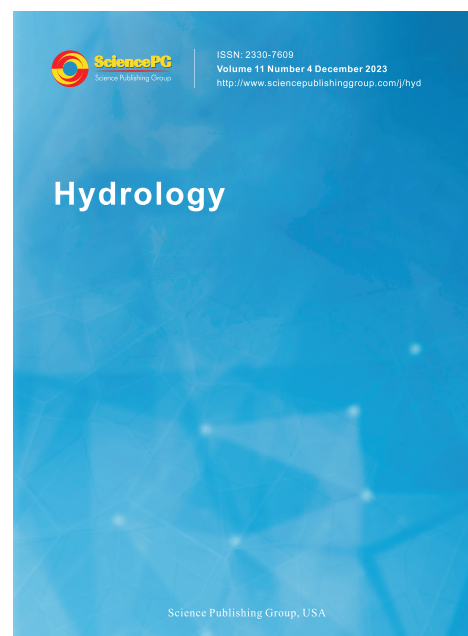
<http://www.sciencepublishinggroup.com/login>

Only the following word processor file formats are acceptable for the manuscript document for all of Science Publishing Group journals: •Microsoft word 2000/2003(doc) •Microsoft word 2007/2010(docx)

Website and Email

<http://www.sciencepublishinggroup.com/j/hyd>

Email: service@sciencepublishinggroup.com



Editorial Board

Dr. Xuezhi Tan	Department of Civil Engineering, Sun Yat-sen University, Guangzhou, China
Qinli Yang	School of Resources and Environment, University of Electronic Science and Technology of China, Chengdu, China
Dr. P. Manju Sree	Advanced Analytics Division, Remote Sensing Applications Area, National Remote Sensing Centre, Indian Space Research Organisation, Hyderabad, India
Dr. Mohammed Bari	Science and Innovation Group, Australian Bureau of Meteorology, West Perth, Australia
Dr. Pushendra Kumar Singh	Department of Water Resources System, National Institute of Hydrology, Roorkee, India
Sirisha Adamala	Department of Natural Resources Management, Indian Council of Agricultural Research-Central Inland Agricultural Research Institute, Port Blair, India
Dr. Vinay Rangari	Department of Civil Engineering, Nanasahab Mahadik College of Engineering, Peth, India
Leila Rahimi	Department of Civil and Environmental Engineering, Politecnico di Milano, Milan, Italy
Ripendra Awal	College of Agriculture and Human Sciences, Prairie View A&M University, Prairie View, United States
Dr. Jichao Sun	School of Water Resource & Environment, China University of Geosciences (Beijing), Beijing, China
Qingwei Zhuang	State Key Laboratory of Information Engineering in Surveying, Mapping and Remote Sensing, Wuhan University, Wuhan, China
Dr. Mohammad Rizwan Jiefeng Wu	Department of Geology, Vikram University, Ujjain, India School of Hydrology and Water Resources, Nanjing University of Information Science and Technology, Nanjing, China
Sabab Ali Shah	Department of Civil and Environmental Engineering, Hanyang University, Seoul, South Korea
Yuhong Li	School of Civil and Hydraulic Engineering, Huazhong University of Science and Technology, Wuhan, China
Dr. Sonam Sandeep Dash	School of Civil Engineering, University College Dublin, Dublin, Ireland
Poojashree B. P.	Department of Marine Geology, Mangalore University, Mangaluru, India
Yuzhen Li	School of Emergency Management, Xihua University, Chengdu, China

ISSN: 2330-7609 (Print), 2330-7617 (Online)



Science Publishing Group (SciencePG), an open access publisher with experienced and eminent reviewers and editorial board members, is mainly attaching importance to developing journals, books and conferences which have owned unique characters respectively. Here is the website of SciencePG: <http://www.sciencepublishinggroup.com>

